Measurement and model analyses of the ozone variation during 2006 to 2015 and its response to emission change in megacity Shanghai, China

Jianming Xu[1,2], Xuexi Tie[3,4], Wei Gao[1,2], Yanfen Lin[5], and Qingyan Fu[5]

[1] Yangtze River Delta Center for Environmental Meteorology Prediction and Warning, Shanghai Meteorological Service, Shanghai, 200135, China
[2] Shanghai Key Laboratory of Health and Meteorology, Shanghai Meteorological Service, Shanghai, 200135, China
[3] Key Laboratory of Aerosol Chemistry & Physics, SKLLQG, Institute of Earth Environment, Chinese Academy of Science, Xi'an, 710061, China
[4] Center for Excellence in Urban Atmospheric Environment, Institute of Urban Environment, Chinese Academy of Science, Xiamen, 361021, China
[5] Shanghai Environmental Monitoring Center, Shanghai, 200135, China

Correspondence: Xuexi Tie (tiexx@ieecas.cn)

Abstract. The fine particles ($PM_{2.5}$) in China decrease significantly in recent years as a result of the implement of Chinese Clean Air Action Plan since 2013, while the O_3 pollution is getting worse, especially in megacities such as Beijing and Shanghai. Better understanding the elevated O_3 pollution in Chinese megacities and its response to emission change is important for developing an effective emission control strategy in future. In this study, we analyze the significant increasing trend of daily maximum O_3 concentration from 2006 to 2015 in the megacity Shanghai with the variability of 0.8-1.3 ppbv yr^{-1}. It is likely attributed to the notable reduction of NO_x concentration with the decreasing rate of 1.86-2.15 ppbv yr^{-1} accompanied with the little change of VOCs during the same period by excluding the weak trends of meteorological impacts on local dispersion (wind speed), regional transport (wind direction) and O_3 photolysis (solar radiation). It is further illustrated by using a state of the art regional chemical/dynamical model (WRF-Chem) to explore the O_3 variation response to the reduction of NO_x emission in Shanghai. The control experiment conducted for September of 2009 shows very excellent performance for O_3 and NO_x simulations including both the spatial distribution pattern, and the day by day variation through comparing with 6 in-situ measurements from MIRAGE-shanghai field campaign. Sensitive experiments with 30% reduction of NO_x emission from 2009 to 2015 in Shanghai estimated by Shanghai Environmental Monitoring Center shows that the calculated O_3 concentrations exhibit obvious enhancement by 4-7 ppbv in urban zones with the increasing variability of 0.96-1.06 ppbv yr^{-1}, which is well consistent with the observed O_3 trend as a result of the strong VOC-limited condition for O_3 production. The large reduction of NO_x combined with less change of VOCs during the past ten years promotes the O_3 production in Shanghai to move towards NO_x-limited regime. Further analysis of WRF-Chem experiments and O_3 isopleths diagram suggests that the O_3 production in downtown is still under VOC-limited regime after 2015 despite of the remarkable NO_x reduction, while moves to the transition regime between NO_x-limited and VOC-limited in sub-urban zones. Supposing the insignificant VOCs variation persists, the O_3 concentration in downtown would keep increasing till 2020 with the further 20% reduction of NO_x emission after 2015 estimated by Shanghai Clean Air Action Plan. The O_3 production in Shanghai will switch from VOC-limited to NO_x-limited regime after 2020 except downtown area which is likely close to the transition regime. As a result the O_3 concentration will decrease by 2-3 ppbv in sub-urban zones, and more than 4 ppbv in suburb response to 20% reduction of NO_x emission after 2020, whereas is not sensitive to both NO_x and VOCs changes in downtown. This result reveals that the control strategy of O_3 pollution is a very complex process, and needs to be carefully studied.

Key Words: O_3 pollution in Shanghai, Long-term O3 trend, WRF-Chem

1 Introduction

Ozone (O_3) in the troposphere plays the important role in the oxidation of chemically and climatically relevant trace gases, hence regulating their lifetime in the atmosphere (Monks et al., 2015). In the lower troposphere, O_3 is produced from photochemical reactions involving volatile organic compounds (VOCs, broadly including CO) and nitrogen oxides (NO_x = NO + NO_2) in the presence of sunlight (Brasseur et al., 1999). As a strong oxidant, O_3 at ground level is detrimental to human health and vegetation (Tai et al., 2014), and has been received continuous attention from both the scientific and regulatory communities in the past three decades.

Shanghai has emerged as one of the largest megacities in the world over the last two decades. The city has a fleet of over 3.6 million vehicles and the population of over 2400 million permanent residents, which results in high emissions of NO_x, VOCs, and primary particulate matter (PM) to the atmosphere from industrial and commercial activities, leading to the photochemical smog formation. Persistent high level of surface O_3 and PM were observed in Shanghai during the past ten years (Geng et al., 2007; Ran et al., 2009; Tie et al., 2009a; Xu et al., 2015). In order to mitigate the adverse impacts from severe air pollution, the Clean Air Action Plan was issued in the end of 2013 to implement the emission reduction program in Shanghai and its neighboring area. As a result, the annual mean $PM_{2.5}$ (particles with diameter $\leqq$ 2.5 μm) mass concentration has decreased from 50 μg m^{-3} in 2013 to 39 μg m^{-3} in 2017. However O_3 pollution has been continuously worsen, with the non-attainment days (daily maximum O_3 concentration exceeding 200 μg m^{-3}, or daily maximum 8h-O_3 concentration exceeding 100 μg m^{-3}) increased from 99 d in 2014 to 129 d in 2016. As a result, O_3 becomes the primary air pollutant affecting the ambient air quality instead of $PM_{2.5}$ in Shanghai. Similar issue has also been occurred in other cities in the eastern China (Lu et al., 2018). For example, the mean $PM_{2.5}$ mass concentration over the 74 major cites decreased by 40% from 2013 to 2017, whereas the maximum daily 8-h average O_3 concentration in summer exceeds the Chinese National Ambient Air Quality Stand (GB3095-2012) over most of eastern China (Li et al., 2019). Thus better understanding the causes of elevated O_3 in China is important for developing effective O_3 control strategies, especially in megacities such as Shanghai.

A prerequisite to an effective emission-based O_3 control strategy is to understand the temporal and spatial relationship between O_3 and its precursors, and the response of O_3 concentrations to the changes in emissions of O_3-precursors (such as NO_x and VOCs, Lin et al., 1988). The relationship of O_3 and O_3-precursors can be clarified as NO_x-limited or VOC-limited chemistry of O_3 formation, which is usually defined based on the relative impact of a given percent reduction in NO_x relative to VOCs in the context of urban chemistry (Sillman, 1999).

Some observational and modeling works on O_3 chemical formation and transformation have been carried out in Shanghai since 2007. The O_3 production in Shanghai city is clearly under VOC-limited regime (Geng et al., 2007), in which the aromatics and alkenes play the dominant roles (Geng et al., 2008a). The aircraft measurements in Yangtze River Delta (YRD) region show the strong anti-correlation between NO_x and O_3 during noontime, indicating the similar VOC-limited regime for O_3 production in the area neighboring Shanghai (Geng et al., 2008b). Thus either NO_x reduction or VOCs growth is favorable for O_3 enhancement in Shanghai. Gao et al. (2017) reported that O_3 concentration in Shanghai downtown increased 67% from 2006 to 2015, whereas NO_x concentration decreased about 38%. This is also consistent with the results of Lin et al. (2017) that, the median of the maximum daily 8-h average O_3 concentration in Shanghai

increased notably from 2006 to 2016, with the rate of 1.4 ppbv yr^{-1}, while the NO_2 decreased from 66.7 to 42.1 $\mu g\ m^{-3}$ with about 20% reduction. These previous studies provide the useful information regarding the O_3 chemical formation and transformation in Shanghai. However, such O_3 variation responding to emission change has not been clearly investigated. Considering that O_3 formation is a complicated process including chemistry, transport, emission, deposition and their interactions, the chemical transport model is the powerful tool to gain an understanding of these interacting processes. For example, Lei et al. (2007), Ying et al. (2009) and Song et al. (2010) investigated the O_3 production rate and its sensitivity to emission changes of O_3 precursors by CAMx model in Mexico City Metropolitan Area (MCMA). Tie et al. (2013) analyzed the comprehensive data of the MIRAGE-Shanghai field campaign by WRF-Chem model, and quantified the threshold value by the emission ratio of NO_x/VOCs for switching from VOC-limited to NO_x-limited in Shanghai. Recently Li et al. (2019) suggested an important cause of the increasing O_3 in North China Plain (NCP) during 2013 to 2017 as the significant decrease in $PM_{2.5}$ slowing down the sink of hydroperoxy radicals and thus speeding up the O_3 production by GOES-CHEM model. However such implication for O_3 trend is not pervasive in YRD and other regions. Moreover, the 5-year O_3 records seem rather short to examine the inter-annual variability of O_3 concentration. The GOES-CHEM experiment with 50 km resolution maybe is suitable for the O_3 simulation at regional scale but is too coarse to resolve the local O_3 budget at urban scale, such as Beijing or Shanghai. To our knowledge, there are no peer-reviewed modeling studies focus on the past long term O_3 variations response to emission changes conducted in Shanghai. Thus this paper extends the study of Tie et al. (2013) and Gao et al. (2017) to not only further examine the inter-annual O_3 variations from a larger scale with more comprehensive measurements, but also explore the O_3 enhancement response to NO_x reduction in Shanghai and predict the future O_3 variations by models. The effects of emission changes on long term O_3 variability are evaluated by WRF-Chem model with high resolution and compared with measurements. The shift of O_3 photochemical regime relative to the variations of NO_x and VOCs concentrations in the past ten years is discussed by O_3 isopleths diagram combined with WRF-Chem model to provide more insights into the O_3 control strategy. Moreover, the future O_3 levels and its possible chemical regime in Shanghai are also discussed according to the Shanghai Clean Air Action Plan.

The paper is constructed as follows. The measurements and models used for this study are described in Sect. 2. The analysis on the long-term in-situ measurements of O_3 and its precursors, as well as the model sensitive experiments are presented and discussed in Sect. 3-6. The conclusion is summarized in Sect. 7.

2 Measurements and models

2.1 Measurements

The measurements of O_3 and NO_x are collected from 6 sites (XJH, PD, JS, BS, SS, DT) over Shanghai (Fig. 1 a) under different influence of air pollutant emissions. The XJH site is located at the downtown of Shanghai, which is strongly influenced by emission of transportation. The PD site is located at the sub-urban area near a big park, which is influenced by the mixed emissions of transportation and residential. The JS site is located in the south of Shanghai with several large chemical industries. The BS site is located in the north of Shanghai with some big steel and power

plants. The SS site is located at the top of the sole hill (100 m a.g.l) in Shanghai, which has minor effect from local emissions, and is influenced by regional transport. The DT site is located at a remote island without anthropogenic activities. These O_3 and NO_x measurements are used for the evaluation on WRF-Chem performance. In addition, the VOCs are sampled at the downtown site XJH and the sub-urban site PD, and are analyzed at a chemistry laboratory. The study on the O_3 chemical production in this paper is limited at XJH and PD by the intensive measurements of O_3 and its precursors (VOCs and NO_x) from 2006 to 2015. The meteorological measurements including wind speed and direction, solar radiation and temperature are collected at BS site, which is the only climatology observatory in Shanghai. The meteorological measurements in BS are used for international exchange of meteorological data representing Shanghai, sponsored by the World Meteorological Organization (WMO).

2.2 Instruments

O_3 is measured using an EC 9810 Ozone Analyzer, together with a UV photometer, which accurately and reliably measures O_3 concentration in ambient air. The oxides of nitrogen analyzer (EC9841B/ECOTECH) have a heated molybdenum NO_2 to NO converter. The resulting NO concentration is quantified using the chemiluminescence technique. This instrument has automated to set to be zero, and include an optional external valve manifold and external calibration sources. Quality control checks are performed every 3 days, including inspection of the shelter and instruments as well as zero, precision and span checks. Filter is replaced once every two weeks and calibration is made every month. The O_3 concentrations are recorded every 1 min.

VOCs concentrations are sampled for 24 h every day with a 6 L silonite canister with a silonite coated valve (model 29-10622). The internal silonite coating improves long-term VOC storage. The instrument has a large volume to detect volatile chemicals down to low pptv range. Absorption is eliminated by using nupropackless valves and by eliminating teflon tape in the valve stem. These canisters are recognized to meet or exceed the technical specifications required for EP methods TO14-A and TO15. Gases samples are pre-processed using Model 7100 VOC preconcentrator. Samples are analyzed for VOCs using a gas chromatography system (Agilent GC6890) coupled with mass-selective detection (Agilent MSD5975 N) with length of 60 m, diameter of 0.32 mm, and film thickness of 1.0 um. This measurement system can detect VOCs concentrations down to low pptv range.

These instruments to measure O_3, NO_x and VOCs concentrations are calibrated carefully. Detail information for the instruments and the procedures to perform data quality control are described by Geng et al. (2007), Ran et al. (2009), Tie et al. (2013) and Gao et al. (2017). These data have been widely used to investigate the diurnal, seasonal and inter-annual variations of O_3 in Shanghai (Geng et al., 2007; 2015; Tang et al., 2008; Ran et al., 2009; Gao et al., 2017) and its chemical mechanism (Geng et al., 2008a; 2008b; Tie et al., 2009a; 2013).

2.3 WRF-Chem model

The regional chemical/transport model (Weather Research and Forecasting Chemical model-WRF-Chem) (Grell et al., 2005) is used to investigate the O_3 variations response to emission changes in Shanghai. The version of the model is improved mainly by Tie et al. (2007) and Li et al. (2010; 2011). The chemical mechanism chosen in WRF-Chem is the RADM2 (Regional Acid

Deposition Model, version 2) gas-phase chemical mechanism (Stockwell et al., 1990), which includes 158 reactions among 36 species. The fast radiation transfer module (FTUV) is developed and used to calculate photolysis rates (Tie et al., 2003), considering the impacts of aerosols and clouds on the photochemistry (Li et al., 2011). The aerosol modules are developed by EPA CMAQ (version 4.6) (Binkowski and Roselle, 2003). The wet deposition of chemical species is calculated using the method in the CMAQ module and the dry deposition parameterization follows Wesely et al. (1989). The ISORROPIA version 1.7 is used to calculate the inorganic aerosols (Nenes et al., 1998). The secondary organic aerosol (SOA) is predicted using a non-traditional SOA module, including the volatility basisset (VBS) modeling approach in which primary organic components are assumed to be semi-volatile and photochemically reactive and are distributed in logarithmically spaced volatility bins. The partitioning of semi-volatile organic species is calculated supposing the bulk gas and particle phases are in equilibrium and all condensable organics form a pseudoideal solution. Nine surrogate species with saturation concentrations from 10^{-2} to 10^{6} $\mu g\ m^{-3}$ at room temperature are used for the primary organic aerosol (POA) components. The SOA contributions from glyoxal and methylglyoxal is also included. The major physical processes employed in WRF are summarized as the Lin microphysics scheme (Lin et al., 1983), the Yonsei University (YSU) PBL scheme (Hong et al., 2006), the Noah Land surface model (Chen and Dudhia, 2001), and the long wave radiation parameterization (Dudhia, 1989).

The domain is set up to covered a region (centered at 32.5°N, 118°E) of 356×345 grids with a horizontal resolution of 6 km (Zhou et al., 2017). The initial and lateral boundary conditions of the meteorology are extracted from the NCEP FNL reanalysis data. The lateral meteorological boundary is updated every 6 h. The chemical lateral boundary conditions are constrained by the global chemical transport model (MOART–Model for Ozone and Related chemical Tracers) with aerosol formation modules (Tie et al., 2001; Emmonset al., 2010). Both the chemical and dynamical integration step is set as 60 s. The Multi-resolution Emission Inventory for China (MEIC) developed by Zhang et al. (2009) is used in WRF-Chem for the domain except Shanghai with 0.25^{o} resolution. The anthropogenic emissions (including CO, NO_x, SO_2 and VOCs) for Shanghai are developed by Tie et al. (2013) with 0.16^{o} resolution based on the MIRAGE-shanghai field campaign. NO_x and SO_2 emissions in YRD region are adjusted by Zhou et al. (2017) according to the performance evaluation of WRF-Chem prediction for about 195 cities during 2014-2015. The distribution of NO_x emission in 2009 in Shanghai is depicted in Fig. 1b. The biogenic emissions are calculated online using the MEGAN (Model of Emissions of Gases and Aerosol from Nature) model developed by Guenther et al. (2006).

Figure 1. (a) The distribution of land-use category in Shanghai. The blue dots denote the locations of 6 sties (XJH, BS, PD, SS, JS, DT). (b) The NO_x emission of 2009 scenario in Shanghai.

2.4 OZIPR model

The ozone isopleths diagram for Shanghai is plot by OZIPR (Ozone Isopleths Plotting Package Research) model (Gery and Crouse, 2002). The OZIPR model employs a trajectory-based air quality simulation model in conjunction with the Empirical Kinetics Modeling Approach (EKMA) to relate O_3 concentrations levels of organic and nitrogen oxide emissions. OZIPR simulates complex chemical and physical processes of the lower atmosphere through a trajectory model. The physical representation is a well-mixed column of air extending from the ground to the top of

the mixed layer. Emissions from the surface are included as the air column passes over different emission sources, and air from above the column is mixed in as the inversion rises during the day. O_3 precursor concentrations and ambient information such as temperature, relative humidity and boundary layer height from measurements in Shanghai were specified for each single run. Therefore a series of simulations were performed to calculate peak O_3 concentration as a function of initial precursor concentrations (Tang et al., 2008; Geng et al., 2008b).

3 Variability of O_3 and its precursors measured in Shanghai

3.1Variation of O_3 concentration

Fig. 2a and b show the annual variation of daily maximum O_3 concentration at downtown site XJH and sub-urban site PD respectively from 2006 to 2015. The daily maximum O_3 concentrations increase notably during the past ten years with the increasing rate of 0.808 ppbv yr^{-1} at XJH and 1.374 ppbv yr^{-1} at PD respectively. In similar the daily maximum 8h-O_3 concentration also increased at the rate of 1.06 and 1.4 ppbv yr^{-1} respectively. It is consistent with the reported O_3 increasing trend ranging from 1-2 ppbv yr^{-1} at background and urban sites in eastern China during 2001 to 2015 (Tang et al., 2009; Ma et al., 2016; Sun et al., 2016). In 2006, the mean daily maximum O_3 concentrations at XJH and PD are 25.2 ppbv and 32.7 ppbv respectively. While in 2017, the mean daily maximum O_3 concentrations at the two sites increase to 41.3 ppbv and 51.8 ppbv respectively, with 64% and 58% enhancement compared with that in 2006. The mean daily maximum O_3 concentration at downtown site XJH during 2006 to 2015 is 39.2 ppbv, which is significantly lower than that at sub-urban site PD of 50.7 ppbv, suggesting the O_3 is depressed in downtown area. Geng et al. (2007) suggested that the O_3 production in the city of Shanghai was under VOC-limited regime, thus higher NO_x in downtown resulted in lower O_3 concentration. Considering the inhomogeneous spatial distribution of the precursors of O_3 in Shanghai (Geng et al. 2008a), we extend the analysis on O_3 variations to a broader scope by using the O_3 measurements from 31 sites provided by Shanghai Environmental Monitoring Center, covering the entire Shanghai area. It is shown in Fig. 2c that the median of the O_3-8h concentration also increases significantly from 2006 to 2015, with the increasing rate of 1.571 ppbv yr^{-1}, indicating that the significant increasing trend of O_3 concentration not only occurs in the city of Shanghai, but also expanded to a larger area nearby Shanghai. Li et al. (2019) also reported a regional O_3 increasing phenomena in summer during 2013 to 2017 from Shanghai to Beijing in eastern China.

In order to analyze the individual contribution to the long-term O_3 trend, the variations of O_3 precursors, and meteorological parameters are measured and showed in the following sections.

Figure 2. The annual variation of daily maximum O_3 concentration (ppbv) from 2006 to 2015 at (a) downtown site XJH and (b) sub-urban site PD, both presenting the significant increasing trends with 0.808 ppbv yr^{-1} at XJH and 1.374 ppbv yr^{-1} at PD. The variation of the median 8-h O_3 concentration (ppbv) from 2006 to 2015 averaged for 31 sites over Shanghai (c), also shows the increasing variability of 1.571 ppbv yr^{-1}.

3.2 Variations of the precursors (NO_x and VOCs)

It is well known that the tropospheric O_3 formation is throughout a complicated photochemical process, and is strongly related to the precursors of O_3 (VOCs and NO_x). According to the previous

studies (Geng et al., 2007; Ran et al., 2009), the chemical formation of O_3 in Shanghai is revealed to be under VOC-limited. Thus either enhancement of VOCs or reduction in NO_x would both result in the growth of O_3 concentration. In order to better understanding the factors possibly driving the O_3 increasing trend depicted in Fig. 2, the variations of NO_x and VOCs concentrations at XJH and PD in the same period are presented in Fig. 3. The NO_x concentrations present significant decreasing trend from 2006 to 2015 at both XJH and PD sites, which is opposite to the increasing trend of O_3 variations in Fig. 2. At XJH, the decreasing rate of NO_x is 2.15 ppbv yr^{-1}, which is more remarkable than that at PD site of 1.86 ppbv yr^{-1}. According to the studies by Lin et al (2017), the reduction of NO_x concentration in Shanghai was likely attributed to the implementation of stringent emission control strategy for transportation, including improvement of gas quality, popular usage of electricity cars, and limitation of heavy cars into the urban zones. These regulations significantly decrease the emissions of NO_x into the atmosphere, resulting in lower NO_x concentrations. Zheng et al. (2018) also reported the 30% reduction of NO_x emission in the past 5 years in YRD region. In comparison, the VOCs concentrations at XJH and PD decrease very slightly during 2006 to 2015. At XJH, the mean VOCs concentration during 2013 to 2015 is about 20 ppbv, which is some lower than that during 2009 to 2012 of 23 ppbv. At PD, the VOCs concentration shows strong inter-annual variations, ranging from 16 to 22 ppbv. Generally the VOCs concentration at the downtown site XJH is higher than that at the sub-urban site PD by 14%. It is consistent with the studies of Cai et al. (2010), suggesting that about 25% of VOCs is attributed to the vehicles in shanghai urban zones.

Figure 3. The mean annual concentrations (ppbv) of NO_x (dots) and VOCs (bars) from 2006 to 2015 at (a) downtown site XJH and (b) sub-urban site PD respectively. The NO_x concentrations at XJH and PD both present obvious decreasing trends with -2.1 ppbv yr^{-1} and -1.87 ppbv yr^{-1}. While the VOCs concentrations at both sites present no clear inter-annual trends.

3.3 Meteorological impacts on O_3 photolysis, dispersion and transport

In addition to the precursors, meteorology such as solar radiation and wind speed and directions also plays the important roles in O_3 concentration through the photochemical and physical processes. Fig. 4 shows the annual variation of wind speed and total solar radiation from 2006 to 2015. The solar radiation presents weak annual variations ranging from 140 to 150 Wm^{-2}, exhibiting a large variability but without a significant trend. As a result, the variation of solar radiation cannot explain the significant change of O_3 concentration on the view of photolysis. The wind speed is usually regarded as the indicator for the dispersion capacity for air pollutants. Several studies reported that the wind speed in winter in eastern China presented decreasing variability during the past 40 years due to the decadal variation of winter monsoon affecting the haze occurrence (Wang et al., 2016; Zhao et al., 2016; Xu et al., 2017). While high O_3 events usually occur in summer season for middle-latitude cities such as Shanghai (Wang et al., 2017). The mean summer wind speed in Fig. 4a fluctuates between 3.3 ms^{-1} to 3.9 ms^{-1} during 2006 to 2015 except the minimum value in 2014 (2.9 ms^{-1}) due to fewer typhoon in the period. Without 2014, the variability of summer wind speed is insignificant, with a trend of -0.02 m s^{-1} yr^{-1}, which could not be regarded as the dominant factor to interpret the increasing O_3 trend. Local O_3 concentration would be affected by transport of upstream plumes usually determined by wind

direction. Geng et al. (2011) suggested that O_3 concentration was higher in west wind compared with other wind sectors in Shanghai indicating the possible O_3 transport from western area out of Shanghai. Fig. 5 presents the annual wind rose at Baoshan site from 2006 to 2015, presenting the very similar pattern of wind direction in each year. The mean wind direction concentrates in the sector between 60-80 degree, suggesting the dominant wind in Shanghai is easterly accounting for 50%. The east wind in Shanghai usually carries with the clean air mass from the sea to improve the local air quality (Xu et al., 2015). The frequency of west wind changes little during 2006 and 2015 ranging from 10-15%, suggesting that the regional transport is not a major factor driving the O_3 increasing. Based on the above analysis, it is speculated that the rapid O_3 increasing during 2006–2015 in shanghai is likely attributed to the reduction of NO_x concentration as a result of the VOC-limited condition for O_3 production.

Figure 4. The annual variation of (a) summer wind speed (m s^{-1}) and (b) total solar radiation (W m^{-2}) from 2006 to 2015 in Shanghai. Both wind speed and the solar radiation present weak inter-annual variations but without significant trends.

Figure 5. The wind rose in each year from 2006 to 2015 in Shanghai. The red line means the resultant vector suggesting the dominant wind direction.

3.4 Different O_3 variability in nighttime and daytime

The mean diurnal variations of O_3 concentrations between 2006 and 2015 are compared in Fig. 6a at XJH and PD sites respectively. The maximum and minimum O_3 concentrations occur in the afternoon (14-15 pm) and early morning (6-7 am) respectively at both sites. In addition, the diurnal O_3 concentrations at XJH and PD sites all increase significantly from 2006 to 2015. For example, the peak O_3 concentration at XJH increases from 21 ppbv to 37 ppbv, meanwhile the minimum O_3 concentration rises from 5 ppbv to 14 ppbv, exhibiting higher increasing rate. Similar diurnal O_3 enhancement is also observed at PD site during the same period. The O_3 chemical mechanism in daytime includes both production and loss processes. In contrast, in nighttime, the photochemical production ceases, and there mainly exists loss process for O_3. In addition both dry deposition and nighttime turbulence also have the influence in the nighttime O_3 concentration according to the work by Hu et al. (2013). Fig. 6b shows the annual change rate of the diurnal O_3 concentration from 2006 to 2015 at XJH and PD sites respectively. The O_3 concentrations present increasing trends both in daytime (8:00-18:00, LST) and nighttime (19:00-07:00, LST) at XJH and PD sites, which is consistent with the results in Fig. 2. The nighttime O_3 concentrations increase more significantly than daytime O_3 at XJH, with the increasing rate of 1.239 and 0.956 ppbv yr^{-1} respectively. While at PD site the O_3 concentrations increase by 1.338 ppbv yr^{-1} in daytime which is higher than that in nighttime by 1.028 ppbv yr^{-1}. In comparison, the nighttime O_3 concentrations exhibit higher increasing rate at downtown site XJH than that at sub-urban site PD due to more NO emissions or more intensified urbanization (Hu et al., 2013) at urban center. These results suggest that the reduction of NO_x concentration from 2006 to 2015 has different effects on daytime and nighttime O_3 variations. The O_3 concentration in nighttime is more sensitive to NO_x reduction at downtown site, resulting in less O_3 lost compared with that in daytime. The results in Fig. 6b also show that the increasing rate of nighttime O_3 in downtown

site XJH is higher than that at sub-urban site PD due to the more reduction of NO_x concentration in downtown area. Furthermore, the seasonal variability of daytime and nighttime O_3 concentrations at XJH site are illustrated in Fig. 7. Both daytime and night O_3 concentrations present increasing trends in all seasons. In comparison, the larger increasing rates of nighttime O_3 concentration are observed in spring, summer and autumn than that in daytime. For example, the nighttime O_3 concentrations increase at 1.341, 1.159 and 1.525 ppbv yr^{-1} in spring, summer and autumn respectively, which are more significant than that of 1.008, 0.378 and 1.370 ppbv yr^{-1} in daytime. The variability of winter O_3 concentrations in daytime and nighttime are generally close perhaps due to the lower O_3 photochemical productions. Hu et al. (2016) suggested that the nighttime boundary layer tended to be less stable resulted from the enhanced sensible heat flux in urban area, thus leading to more active nighttime turbulence. The sounding measurements at 20:00 (LST) in Shanghai are used to calculate the vertical temperature gradient between 1000 hPa and 925 hPa to indicate the intensity of nighttime turbulence, while presenting no significant trend from 2010 to 2015. Furthermore the PBL height retrieved from Lidar measurements at 20:00 (LST) presents the similar results as soundings. Based on the above measurements, the variation of turbulence at night may have only minor contribution to the nighttime O_3 increasing in Shanghai. However the effect of dry deposition could not be excluded by lacking of measurements, which need further investigation.

Figure 6. (a) The mean diurnal variation of O_3 concentration (ppbv) compared between 2006 and 2015 in XJH (red dots) and PD (blue dots). (b) The annual change rate of diurnal O_3 concentration (ppbv.yr^{-1}) from 2006 to 2015 at downtown site XJH (red bars) and sub-urban site PD (blue bars).

Figure 7. The daytime (8:00-18:00, LST) and nighttime (19:00-07:00, LST) O_3 variability from 2006 to 2015 at downtown site XJH in (a) spring, (b) summer, (c) autumn and (d) winter.

4 WRF-Chem study on the O_3 variation response to emission change

4.1 Design of the model experiments scheme

To better understand the role of NO_x emission reduction in O_3 variation, the WRF-Chem model is utilized to calculate the changes of O_3 concentrations. Lin et al. (2017) suggested that the NO_x emission was reduced in Shanghai in recent years resulted from the implementation of the Shanghai Clean Air Action Plan. The NO_x emission in 2015 is estimated at 33.4×10^4 ton in Shanghai, reduced significantly by 30% compared with that in 2009 of 44.9×10^4 ton. Thus it provided the good opportunity to examine the O_3 variation response to the reduction of NO_x emission in Shanghai. The NO_x emissions in 2009 and 2015 are put into WRF-Chem model respectively to calculate the O_3 concentration. The other emissions (including gas and particulate matter) and meteorology used in WRF-Chem are set to be same. As a result, the difference of O_3 concentrations calculated by WRF-Chem is solely attributed to the change of NO_x emission between 2009 and 2015, which is furthermore compared with the measurements.

The MIRAGE-shanghai field campaign was conducted in September of 2009 to explore the O_3 chemical formation and transformation in Shanghai (Tie et al., 2013). The mean temperature, mean wind speed and total precipitation in this month is 25 ^oC, 2.85 m s^{-1} and 89.5 mm respectively, which is very close to the climatological conditions during the past ten years from

2006 to 2015, with 24.7 ^{o}C for mean temperature, 2.81 m s^{-1} for mean wind speed, and 126 mm for total precipitation respectively. In addition, Shanghai is located at the typical sub-tropical area. The meteorology in September is characterized as the low cloud cover and rain occurrence, the slight wind speed and humidity, as well as the moderate solar radiation intensity. As suggested by Tie et al. (2013), the chemical age of O_3 plume in Shanghai urban area in September of 2009 was very young, indicating that the O_3 production was more dependent on the local emissions under such kind of meteorology, hence providing more insights into the O_3 chemical mechanism response to the local emission changes. We chose the meteorology in September of 2009 as the atmospheric background for all the sensitive experiments by WRF-Chem.

Tie et al. (2009a; 2013) highlighted that the WRF-Chem model was capable of studying the chemical and physical processed of O_3 in September of 2009 during the MIRAGE-Shanghai campaign. The calculated O_3, NO_x, VOCs and aerosols by WRF-Chem in clean and polluted episodes are fairly in agreement with the measurements except HONO, suggesting that the emission inventory in 2009 used in the model is reasonable for the Shanghai region. Moreover the VOCs emission in Shanghai is greatly improved according to the measurements from the MIRAGE-shanghai field campaign by Tie et al. (2013). Such emission from Tie et al. (2013) representing 2009 scenario is used in this study to conduct the control experiment (T1) as the baseline to simulate the O_3 and NO_x concentrations in September of 2009. The T1 experiment is composed of 30 model runs for each day in September of 2009. Each model run is initiated at the 20:00 (LST) and performed for 52 h integrations. The first 28 h integration is regarded as model spin-up periods, the results from the later 24 h integration is captured hourly and averaged for mean daily concentration of O_3 and NO_x. The aim of the T1 experiment is to further evaluate the reliability of the emission inventory in 2009 used in WRF-Chem by fully comparing the calculated O_3 and NO_x concentrations with in-situ measurements of 6 sites over Shanghai.

4.2 The NOx emission in 2009 used for base experiment

The distribution of NO_x emission of 2009 scenario (Tie et al., 2013) in Shanghai used in WRF-Chem model has been showed in Fig. 1b. The NO_x emission is mostly distributed in the urban zones, suggesting that transportation is the important source. The NO_x is largely exported in downtown and two neighboring sub-urban zones in the east and north respectively. The maximum NO_x emission is estimated at 16 kg hr^{-1} km^{-2} at downtown, compared with 2-6 kg hr^{-1} km^{-2} in the sub-urban area. In addition, there is a small town located in the south of Shanghai with the similar intensity of NO_x emission as the sub-urban zones. The total NO_x emission of 2009 scenario in Shanghai (Fig. 1b) is estimated at 41.4×10^4 ton in the model, which is close to the 47.8×10^4 ton suggested by Lin et al. (2017) according to the Shanghai Environmental Year Book.

4.3 Performance evaluation on the base experiment

The mean daytime and nighttime O_3 concentrations in September 2009 are calculated by WRF-Chem and compared with measurements over 6 sites in Shanghai, which are presented in Fig. 8a and b respectively. Both modeled and measured O_3 concentrations in daytime are higher than that in nighttime. The calculated daytime O_3 concentration is about 10-18 ppbv higher than that in nighttime in urban region, which is consistent with the measured difference of 12-14 ppbv at XJH and PD sites. The observed daytime and nighttime O_3 concentrations at remote site DT show the minimum difference of 5 ppbv which is also captured by WRF-Chem model due to the

less impact of anthropogenic emissions. In Fig. 8a, there exists a large O_3 plume with high concentration of 40-48 ppbv in daytime in the west of Shanghai and its neighboring area from WRF-Chem simulations. It is also illustrated by the daytime O_3 measurements at SS site with 40 ppbv. However such daytime O_3 plume dissipates at night (Fig. 8b) leading to the significant difference of O_3 concentration between day and night. Tie et al. (2013) suggested the enhancement of O_3 concentration in the downwind of Shanghai due to the considerable O_3 formation in the aged city plume transported westerly in September resulted from the dominant west winds. According to the study of Tie et al. (2013), the O_3 concentrations had a minimum within 20 km of the city, and enhanced at the west of 100–150 km away from the city in daytime, which was consistent with the results of daytime O_3 distribution simulated by WRF-Chem in Fig. 8a. In addition, both model simulations and in-situ measurements in daytime and nighttime highlight the lower O_3 concentration in urban zones than that in suburb. The simulated daytime and nighttime O_3 concentration in downtown is 28-32 ppbv and 12-14 ppbv respectively, significantly lower than that at sub-urban (36-38 ppbv and 26-28 ppbv respectively) and rural area (40-42 ppbv and 36-38 ppbv respectively). Similarly, the measured daytime O_3 concentration at downtown site XJH is 28 ppbv, lower than that at sub-urban site PD and remote site DT by 12 ppbv and 21 ppbv respectively. Geng et al. (2007) suggested that under VOC-limited regime, the lower O_3 concentration in downtown was resulted from the higher NO_x emission, which depressed the O_3 production process. Under high NO_x conditions, the OH radicals are lost by the reaction of $NO_2 + OH \rightarrow HNO_3$ (Sillman, 1995). As a result, higher NO_x concentration in urban area leads to lower OH concentration, which results in smaller O_3 production. Tang et al. (2008) also suggested that the O_3 concentration in Shanghai downtown was higher on weekends than that on weekdays due to the reduced NO_x concentration. However the discrepancy is also evident between model results and measurements. For example, the modeled nighttime O_3 concentrations at XJH and PD are about 2-6 ppbv lower than the measurements, perhaps due to the uncertainty of NO_x and VOCs emission in urban area suggested by Tie et al. (2009a). In addition, the calculated daytime O_3 concentrations in the remote site DT and chemical site JS are lower than measurements by 10 ppbv and 6 ppbv respectively. The former is resulted from the overestimation of the wind speed by WRF-Chem model leading to excessive O_3 transport for underestimation (Zhou et al., 2017). While the latter is mainly due to the prominent underestimation of the VOCs emission in the chemical zones suggested by Tie et al. (2009a).

Figure 8. The calculated distribution of (a) daytime and (b) nighttime O_3 concentration by WRF-Chem (shade) in September of 2009 compared with measurements (circles) of 6 sites over Shanghai. The minimum O_3 concentrations in daytime and nighttime both occur in urban center.

Fig. 9a and b show the daily variations of O_3 and NO_x concentrations compared between WRF-Chem simulations and the in-situ measurements over 5 sites. The statistical analysis of model performance for O_3 and NO_x is listed in Table 1 and Table 2 respectively. The calculated magnitude and daily variation of O_3 concentrations agree well with the measurements, suggesting that both meteorology and photochemistry are well reproduced by WRF-Chem model. For example, the Root Mean Square Error (RMSE) calculated between modeled and measured O_3 concentration are 7.4, 10.5, 12, 8.6, 9.2 ppbv for XJH, JS, DT, PD and BS respectively, and the difference between the simulation results and in-situ measurement is below 10%, which are very

satisfactory compare with the similar works by Geng et al (2007) and Tie et al. (2013). The correlated coefficients (R) for the mean daily O_3 concentration range from 0.6 to 0.8 above 99% confidence over 5 sites, indicating good consistency of day by day variations between the model results and measurements. Comparably the O_3 concentration is best simulated by WRF-Chem at the downtown site XJH and sub-urban site PD with the lower RMSE and better R. However the discrepancy of daily O_3 concentration between the model and measurements is also evident. For example, a rapid change of O_3 concentration from 16 to 19 in September was observed over all sites, indicating it's a regional event instead of a local phenomenon. The O_3 concentration firstly increases significantly during 16-19 (episode-1), then sharply decreased during the later 4 days (episode-2). The similar rapid O_3 change in Shanghai was also reported by Tie et al. (2009a), and their explanation is that this episode was mainly related to the intensity of the sub-tropical high-pressure system on Pacific Ocean in summer. The model captures the O_3 variations and magnitudes during the both risen and fallen episodes very well at downtown site XJH, but substantially underestimates the increasing variability of O_3 concentration during episode-1 at sub-urban and rural sites by 10-15 ppbv. Geng et al. (2008a) suggested the "chemical transport of O_3" from Shanghai downtown area to the distance of 18-36 km far away, which increased the O_3 concentration at sub-urban or rural sites. This "chemical transport of O_3" is difficult to be reflected by WRF-Chem model due to the current inventory is too coarse to accurately reflect the detailed distribution and variation of NO_x emission, e.g. the NO_x emission from mobile source in the city. In addition, the underestimation of the O_3 concentration at suburb of Shanghai in summer is possibly attributed to the model bias of sea breeze simulations. Under the condition of weak sub-tropical pressure, the sea breeze develops at noontime to yield a cycling wind pattern in Shanghai, leading to the rapid accumulation of high O_3 concentration. The WRF-Chem usually underestimates the sea surface temperature, which tends to accelerate the sea breeze development and weak the O_3 trapping in the city (Tie et al., 2009a). The calculated daily NO_x concentration by WRF-Chem compared with measurements are shown in Fig. 9b. Both the modeled and measured NO_x concentrations at the remote site DT are very low, with the average of 1.4 and 2.9 ppbv respectively due to seldom anthropogenic emissions there. The calculated NO_x concentration at XJH and PD are generally well consistent with the measurements with the excellent R of 0.8 and 0.82 and small RMSE of 6.9 and 7.5 ppbv respectively. However the NO_x concentration is underestimated by WRF-Chem at sub-urban site BS in the steel zone. The calculated NO_x concentration at BS is 16.1 ppbv, which is lower than the measurements by 5 ppbv. The difference of NO_x concentrations between the model and observations is generally above 10%, suggesting the performance of NO_x simulation is somewhat lower than that of O_3. It was also reported by Tie et al. (2007; 2009b; 2013), during the evaluation of the NO_x calculations by WRF-Chem in MIRAGE-Shanghai and MIRAGE-mex campaign studies. The lifetime of NO_x at the surface is about 1-2 days, shorter than O_3. Thus the NO_x concentration is determined by the detailed emissions and dynamical factors, which need to develop the advanced inventory with higher resolution to reproduce both the spatial distributions and temporal variations of NO_x emission.

Figure 9. The calculated mean daily concentrations (ppbv) of (a) O_3 and (b) NO_x at 5 sites in September of 2009 by WRF-Chem (red circles) and compared with measurements (blue circles).

4.4 Sensitive study on the O_3 variability response to the emission change

The T1 experiment shows the excellent performance for O_3 and NO_x simulations, including the spatial distribution pattern, and the day by day variation and magnitude. It is indicated that the emission in 2009 scenario used in WRF-Chem is reasonable, and the model is efficient for conducting the sensitive studies on O_3 variation response to the emission change. In order to better understand the measured long-term trend of O_3 concentration during the past ten years in Shanghai and its relationship to the emission reduction, several sensitive studies are conducted in this study (Table 3). The control study of T1 is conducted based on the NO_x emission in 2009 scenario in Shanghai. According to the study of Lin et al. (2017), the NO_x emission in 2015 in Shanghai is reduced by 30% compared with that in 2009. Thus we conduct the sensitive experiment T2 by WRF-Chem, cutting the NO_x emission by 30% compared with T1, whereas keeping the other emissions and meteorology same as T1. As a result, the calculated O_3 difference between T1 and T2 is likely attributed to the NO_x emission reduction between 2015 and 2009.

Fig. 10a shows the distribution of the difference of O_3 concentration simulated by T1 and T2 (T2-T1). The reduction of NO_x emission has the obvious effect on the magnitude and distribution of O_3 concentration. The O_3 concentration increases notably in urban area corresponding to the higher NO_x emissions in Fig. 1, ranging from 2-7 ppbv. The enhancement of O_3 concentration is most significant in downtown and neighboring sub-urban zones, as well as the southern town, generally more than 4 ppbv. For example, the maximum increase in O_3 concentration is 6.4 ppbv occurred at downtown site XJH, followed by 4-5 ppbv at sub-urban site PD. The increasing rates of O_3 trend at XJH and PD are estimated at 1.06 ppbv yr^{-1} and 0.96 ppbv yr^{-1} from 2009 to 2015 by WRF-Chem, which is consistent to the observed O_3 growth variability of 1-1.3 ppbv yr^{-1}. The response of O_3 concentration to the NO_x reduction is not evident in the rural area including the eastern part of Shanghai and the island with low NO_x emissions. The comparison of T1 and T2 further illustrates the speculation that the significant increasing trend of O_3 concentration during the past ten years in Shanghai is mostly attributed to the reduction of NO_x emission as a result of the implementation of Shanghai Clean Air Action Plan.

The O_3 chemical formation is strongly related to NO_x and VOCs concentrations. As discussed by Geng et al. (2008a) the O_3 chemical formation is clearly under VOC-limited regime in Shanghai and its neighboring area. Under the high NO_x condition, NO tends to react with O_3 instead of NO_2, flowing by $NO_2 + OH \rightarrow HNO_3$, causing the decrease of the reactivity and ensuing O_3 concentrations. Thus reduced NO_x emission would result in increase in O_3 concentration, which has been discussed in Fig. 10a.

Despite of minor change of VOCs in the last ten years, it is worth to investigate the effect of the VOCs changes on O_3 concentrations in Shanghai. For this purpose, we conduct a sensitive study (T3), with 50% increase of VOCs emission compared with T1, but keeping NO_x and other emissions as well as the meteorology same as T1. For RADM2 gas mechanism used in WRF-Chem, the VOCs are surrogated into 14 species, such as alkane, alkene, aromatic, formaldehyde, etc. All the species of VOCs are increased by 50% at every model grid over Shanghai and at every hour. The difference of O_3 concentration between T3 and T1 (T3-T1) is shown in Fig. 10b. As we expected, the O_3 concentration in Shanghai is sensitive to the enhancement of VOCs emission, increased by 3-4 ppbv in urban area due to more NO is converted to NO_2 by reaction with RO_2 and HO_2. Furthermore, the abundant O_3 plumes produced in the urban zones significantly

transport to the downwind areas about 100-200 km away, resulting in elevated O_3 concentration in the western Shanghai by about 2 ppbv. According to Tie et al. (2013), the O_3 plume released in Shanghai urban area can be transported to downwind of the city by about 100-150 km away in the MIRAGE-shanghai field campaign. The model studies of T1, T2 and T3 highlight that under the emission of 2009 scenario, the O_3 chemical production is clearly under VOC-limit regime, either decreasing NO_x concentration or increasing VOCs concentration would result in the O_3 enhancement. The analysis on in-situ measurements and model experiments jointly suggests that the significant O_3 increasing trend during the past ten years in Shanghai is mainly attributed to the large reduction of NO_x emission.

Figure 10. The difference of O3 concentration (ppbv) between (a) T2 and T1 (T2-T1), (b) T3 and T1 (T3-T1) respectively conducted by WRF-Chem model. The difference between T2 and T1 lies in the NO_x emissions set in T2 (2015 scenario) is 30% lower than that in T1 (2009 scenario), which is estimated by Lin et al. (2017) according to the Shanghai Environment Yearbook. The difference between T3 and T1 is dependent on that the VOCs emission in T3 is 50% higher than that in T1.

4.5 The variation of O_3 production regime response to emission change

The O_3 chemical mechanism in Shanghai was explored by several studies based on the in-situ measurements around 2008 and 2009. Geng et al. (2008a; 2008b), Ran et al. (2009) and Tie et al. (2009a) all revealed that the O_3 production around 2008 and 2009 in Shanghai was clearly under VOC-limit regime which was further illustrated by the above model studies. As indicated in Fig. 3, the significant decrease of NO_x concentration is observed from 2009 to 2015 in Shanghai, while the VOCs concentration changed little during the same period. As we know, the O_3 chemical formation is strongly related to NO_x and VOCs concentrations with nonlinearity. Thus the different variability of NO_x and VOCs concentration from 2009 to 2015 inevitably has the large effect on the O_3 production regime, which need to be investigated deeply.

The complex relationship among NO_x, VOCs and O_3 concentrations is usually depicted by O_3 isopleths diagram. The O_3 isopleths plot (Fig. 11) in Shanghai used in this study is constructed by the OZIPR model based on the in-situ measurements of O_3, NO_x, VOCs and meteorology. Under high VOCs and low NO_x condition (low NO_x/VOCs ratio), the O_3 production is not sensitive to VOCs, while positively correlated to NO_x concentration, which is viewed as NO_x-limited regime. By contrast, under low VOCs and high NO_x condition (high NO_x/VOCs ratio), the O_3 production tends to increase with the VOCs growth or NO_x reduction, which is regarded as VOC-limited regime. The NO_x-limited and VOC-limited regime is divided by a ridge line (the dot-dash line in Fig. 11) in the O_3 isopleths plot. The O_3 production is not sensitive to neither NO_x concentration nor VOCs concentration when near the ridge line, which is regarded as the transition regime.

The O_3 chemical production regime at XJH and PD in 2009 and 2015 is positioned respectively in Fig. 11. In 2009 the O_3 production at both XJH and PD sites (marked as red and blue hollow circle respectively) are clearly under VOC-limited regime. Thus decrease in NO_x concentration leads to the O_3 enhancement, which is highlighted by the previous in-situ measurements and model experiments. Since then the O_3 production regime tends to move toward the dot-dash line due to the significant reduction of NO_x concentration accompanied with the relative less change of VOCs at the two sites. In 2015 the O_3 production at XJH (marked as red

solid circle) is still under VOC-limited regime, but for PD (marked as blue solid circle), it is close to the dot-dash line, approaching the transition regime between VOC-limited to NO_x-limited. This result suggests that if the NO_x emission keeps reduction after 2015 assuming the VOCs concentration keeps constant, the O_3 concentration will continue to increase at XJH, while at PD the O_3 concentration is supposed to be insensitive to the NO_x change. According to the O_3 chemical regime depicted in Fig. 11, if the NO_x concentration decreases by 5 ppbv after 2015, the peak O_3 concentration at XJH will further increase by 3 ppbv, whereas at PD it seems to change very slightly. To better understand this further change, more sensitive studies of WRF-Chem are conducted in the following sections.

Figure 11. The O_3 chemical production at downtown site XJH and sub-urban site PD in 2009 and 2015 depicted by O_3 isopleths diagram. The hollow and solid red circles denote O_3 production regime at XJH in 2005 and 2019 respectively. The hollow and solid blue circles denote O_3 production regime at PD in 2005 and 2019 respectively

5 The future O_3 evaluation

5.1 The O_3 level in 2020

According to the Shanghai Clean Air Action Plan, the NO_x emission in Shanghai will be further reduced by 20% in 2020 compared with that in 2015. According to the above analysis based on the O_3 isopleths plot (Fig. 11), the O_3 concentrations in downtown and sub-urban seem to have distinct different responses to further NO_x reduction after 2015. In order to better understand the future O_3 variation, the sensitive experiment T4 is conducted by WRF-Chem with 20% reduction of NO_x emission compared with T2. T2 and T4 represent the NO_x emission in 2015 and 2020 respectively. The other emissions and meteorology are set to be same as T1. The difference of O_3 concentration between T2 and T4 (T4-T2) is presented in Fig. 12a. The O_3 concentration keeps increasing in downtown area such as XJH site, ranging from 2-4 ppbv. However, for the sub-urban zones such as the PD site, the O_3 concentration changes very little response to the further NO_x reduction, ranging from 0-1 ppbv. As discussed in Fig. 11, in 2015 the O_3 production at PD is possibly under the transition regime from VOC-limited to NO_x-limited near the ridge line. As a result, the O_3 concentration is not sensitive to the variation of NO_x concentration. However the O_3 concentration in the suburb zones generally decreases by 1ppbv, indicating that with the further NO_x reduction after 2015 the O_3 chemical production transfers from VOCs-limited to NO_x-limited regime in the rural of Shanghai.

It is suggested in Fig.11 that the O_3 production at downtown site XJH in 2015 is still under VOC-limited regime despite of the significant NO_x reduction. The O_3 concentration would be also sensitive to the variation of VOCs concentration. Thus the sensitive experiment T5 is conducted by WRF-Chem model with 50% enhancement of VOCs emission compared with T2 (representing the emission in 2015 scenario). It is presented in Fig. 12b that the O_3 concentration increases by 2-3 ppbv in downtown area due to the enhancement of VOCs, suggesting that the O_3 production at downtown in 2015 is still under VOC-limited regime, which is consistent with the results in Fig. 11. Moreover the O_3 plumes produced in urban area transport to the downwind area to accumulate the high O_3 concentration in the western area to Shanghai by 2 ppbv. While at sub-urban site PD, the O_3 concentration changes less than1 ppbv response to the increase in

VOCs emission, which is similar as the very weak O_3 variations relative to the NO_x reduction in Fig. 12a. Overall, the models studies of T4 and T5 jointly suggest that the O_3 concentration at sub-urban site PD in 2015 is not sensitive to either NO_x or VOCs variations due to the O_3 production is under the transition regime depicted in the O_3 isopleths plot.

Figure 12. The difference of O3 concentration (ppbv) between (a) T4 and T2 (T4-T2), (b) T5 and T2 (T5-T2) respectively conducted by WRF-Chem model. The difference between T4 and T2 is that the NO_x emissions set in T4 (2020 scenario) is 20% lower than that in T2 (2015 scenario), which is estimated according to the Shanghai Clean Air Action Plan. The difference between T5 and T2 lies in that the VOCs emission in T5 is 50% higher than that in T2.

5.2 The O_3 chemical production after 2020

The above study shows that the O_3 production at sub-urban site PD in 2020 will likely transfer from VOCs-limited regime to NO_x-limited regime without consideration of possible VOCs changes. For the purpose of the O_3 pollution control strategy, it is worth to estimate the O_3 level response to emission change after 2020 in Shanghai. It is also essential to access how many NO_x emission need to be cut after 2020 will cease the O_3 enhancement in downtown area. Thus the sensitive experiment T6 is conducted by further 20% reduction of NO_x emission from 2020 scenario (T4). The difference of O_3 concentration between T6 and T4 (T6-T4) is shown in Fig. 13a. It is clear that the O_3 concentration at downtown keeps nearly constant regardless of the further reduction of NO_x emission after 2020. That is to say the increasing trend of O_3 in downtown with the NO_x reduction ceases after 2020, indicating that the O_3 production likely approachs the transition regime. In addition, the O_3 concentration decreases significantly out of the downtown area, ranging from 2-3 ppbv in sub-urban zones, and more than 4 ppbv in suburb, indicating that the O_3 production in Shanghai transfers to NO_x-limited regime after 2020 except the downtown area where the O_3 production is likely near the transition zone. On the other hand, if the NO_x emission is kept constant after 2020 as T4, while the VOCs emission is increased by 50% conducted in T7 experiment, the O_3 concentration (Fig. 13b) changes little in both urban and suburb area in Shanghai which is different from the previous model study of T5 the T3 when O_3 production is under VOC-limited condition. It is suggested that the O_3 concentration after 2020 is not sensitive to the variation of VOCs concentration because the continuous reduction of NO_x emission keeps in promoting the O_3 production to transfer into NO_x-limited regime. Thus further reduction of NO_x tends to decrease the O_3 concentration in Shanghai.

Figure 13. The difference of O3 concentration (ppbv) between (a) T6 and T4 (T6-T4), (b) T7 and T4 (T7-T4) respectively conducted by WRF-Chem model. The NO_x emissions set in T6 is 20% lower than that in T4 (2020 scenario). The VOCs emission in T7 is 50% higher than that in T4.

Conclusions

O_3 pollution is a serious issue in China. Better understanding the elevated O_3 and its response to emission change is important for Chinese megacities. In this study, we analyze the increasing trend of O_3 concentration by long-term measurements of O_3 and its precursors as well as meteorology in Shanghai combined with the WRF-Chem model. The O_3 production regime

response to the emission change in Shanghai during the past ten years is also explored by O_3 isopleths plot. In addition, the future O_3 variation and its chemical production in Shanghai are evaluated by WRF-Chem model. The main conclusions are summarized as follows:

(1) The daily maximum O_3 concentration measured in Shanghai increased significantly from 2006 to 2015 with the rate of 0.808 ppbv yr^{-1} at downtown site XJH and 1.374 ppbv yr^{-1} at sub-urban site PD respectively. The observed increasing trend of O_3 is not limited in the urban zones but expanded to the larger scale covering the total Shanghai city. The NO_x and VOCs concentrations presented different variability from O_3 during the same period, in which NO_x concentration decreases significantly at both XJH and PD sites, whereas the VOCs changes very little without evident trend.

(2) Because there are minor trends of measured O_3 photolysis, local dispersion and regional transport resulted from meteorology, it is speculated that the significant O_3 increasing trend during 2006 to 2015 in Shanghai is likely attributed to the reduction of NO_x concentration as a result of the strong VOCs-limited regime for O_3 production. The nighttime O_3 is more sensitive to NO_x reduction than that in daytime, because of more O_3 is depressed by NO_x in nighttime. As a result, the observed nighttime O_3 concentration at XJH increases more rapidly than that in daytime response to the NO_x reduction.

(3) The WRF-Chem model is utilized to calculate the long term O_3 variations response to emission change. The sensitive experiments illustrate that either reduction of NO_x emission or growth of VOCs emission conducted by WRF-Chem lead to the significant enhancement in O_3 concentration in urban zones in 2009 as the baseline, indicating the O_3 production is clearly under VOC-limited regime. The calculated O_3 concentration increases by 1-7 ppbv in urban zones from 2009 to 2015 resulted from 30% reduction of NO_x emission estimated by Shanghai Environmental Monitoring Center. The enhancement of O_3 concentration is significant in urban zones generally more than 4 ppbv, with the maximum elevation of 6-7 ppbv occurred at downtown area, which is consistent with the measurements. The increasing rates of O_3 trend at downtown site XJH and sub-urban site PD are estimated at 1.06 ppbv yr^{-1} and 0.96 ppbv y^{r-1} from 2009 to 2015 by WRF-Chem, which is close to the observed O_3 growth variability of 1-1.3 ppbv yr^{-1}. This result suggests that the observed increasing trend of O_3 concentration during the past ten years in Shanghai is likely attributed to the reduction of NO_x emission under the VOC-limited condition for O_3 production.

(4) The model sensitive study suggests that significant decrease in NO_x concentration combined with the obscure VOCs variation from 2006 to 2015 gradually promotes the O_3 chemical production in Shanghai from VOC-limited to NO_x-limited, which is consistent with the O_3 isopleths diagram. The O_3 isopleths plot shows that O_3 production is in VOC-limited regime in both downtown site XJH and sub-urban site PD in 2009. With the 30% reduction of NO_x emission from 2009 to 2015 estimated by Shanghai Environmental Monitoring Center, the O_3 production in XJH is still under VOC-limited regime, while the O_3 production moves to the transition regime in PD, suggesting that the O_3 concentration in sub-urban zones is not sensitive to the variation of either NO_x or VOCs concentration.

(5) In order to better understand the O_3 control strategy in Shanghai, the future O_3 production is estimated by WRF-Chem. The O_3 concentration in Shanghai downtown would keep increasing till 2020 with the 20% reduction of NO_x emission after 2015 estimated by Shanghai Clean Air Action Plan. If the NO_x emission is further decreased by 20% after 2020, The O_3

concentration will decrease by 2-3 ppbv in sub-urban zones, and more than 4 ppbv in suburb. While the O_3 concentration in downtown is not sensitive to either NO_x reduction or VOCs enhancement after 2020, indicating the O_3 production in shanghai will transfer to NO_x-limited regimes except downtown where the O_3 production is likely close to the transition regime. Further reduction of NO_x emission after 2020 tend to mitigate the O_3 pollution in Shanghai.

(6) There are some uncertainties and limitations existed in the study. First, the inhomogeneity of the NO_x reduction is not considered in the sensitive experiments by lacking of the high resolution emission inventory (e.g. 1 km resolution). Second, the variation of VOCs emission is not taken into account in the model experiments due to the more uncertainties existed in the current VOCs emission inventory. While O_3 production in Shanghai is very sensitive to some VOC species, especially aromatics. Thus the accurate emission inventory of VOCs need to be developed and included in the future study. Third, the same meteorology is used for all WRF-Chem simulations. However the O_3 photolysis, advection, and vertical diffusion are all strongly affected by meteorology. The change of meteorology would be considered and evaluated in the future studies for more deep investigation.

Data availability. The data used in this paper can be provided upon request from Jianming Xu (metxujm@163.com).

Author contributions. XT came up with the original idea of investigating the impact of emission change on long term O3 variations by. XT and JX designed the analysis method. JX conducted the analysis. WG, YL and QF provided the observational data and helped in discussion.

Competing interests. The authors declare that they have no conflict of interest.

Acknowledgements. This study was funded by the National Key R&D Program of China (grant 2018YFC0213800), the National Natural Science Foundation of China (91644223, 41430424, 41730108 and 41801367).

776 **References**

777 Binkowski, F. S. and Roselle, S. J.: Models-3 community multi scale air quality (CMAQ) model
778 aerosol component – 1. Model description, Journal of Geophysical Research, 108 (D6),
779 4183, doi:10.1029/2001jd001409, 2003.
780 Brasseur, G. P., Orlando, J. J., and Tyndall, G. S.: Atmospheric chemistry and global change, Oxford
781 University Press, Cambridge, USA, 654 pp., 1999.
782 Cai, C. J., Geng, F. H., Tie, X. X., Yu, Q., and An J. L.: Characteristics and source apportionment of
783 VOCs measured in Shanghai, China, Atmospheric Environment, 44, 5005-5014, 2010.
784 Chen, F. and Dudhia, J.: Coupling an advanced land surface hydrology model with the Penn
785 State-NCAR MM5 modeling system, Part I: Model implementation and sensitivity, Monthly
786 Weather Review, 129, 569–585, 2001.
787 Dudhia, J.: Numerical study of convection observed during the winter monsoon experiment using
788 a mesoscale two-dimensional model, Journal of the Atmospheric Sciences, 46, 3077–3107,
789 1989.
790 Emmons, L. K., Walters, S., Hess, P. G., Lamarque, J. F., Pfister, G. G., Fillmore, D., Granier, C.,
791 Aguenther, A., Kinnison, D., Laepple, T., Orlando, J., Tie, X., Tyndall, G., Wiedinmyer, C.,
792 Baughcum, S. L., and Kloster, S.: Description and evaluation of the model for ozone and
793 related chemical tracers, version4 (MOZART-4), Geoscientific Model Development, 3, 43–67,
794 2010.
795 Gao, W., Tie, X. X., Xu, J. M., Huang, R. J., Mao, X. Q., Zhou, G. Q., and Chang, L. Y.: Long-term
796 trend of O_3 in a mega City (Shanghai), China: Characteristics, causes, and interactions with
797 precursors, Science of the Total Environment, 603-604, 425-433, 2017.
798 Geng, F. H., Zhao, C. S., Tang, X., Lu, G. L., and Tie, X. X.: Analysis of ozone and VOCs measured in
799 Shanghai: a case study, Atmospheric Environment, 41, 989–1001, 2007.
800 Geng, F. H., Tie, X., Xu, J., Zhou, G., Peng, L., Gao, W., Tang, X., Zhao, C.: Characterizations of ozone,
801 NO_x, and VOCs measured in Shanghai, China, Atmospheric Environment, 42, 6873–6883,
802 2008a.
803 Geng, F. H., Zhang, Q., Tie, X., Huang, M., Ma, X., Deng, Z., Quan, J., and Zhao, C.: Aircraft
804 measurements of O_3, NO_x, CO, VOCs, and SO_2 in the Yangtze River Delta region, Atmospheric
805 Environment, 43, 584–593, 2008b.
806 Geng, F. H., Tie, X., Guenther, A., Li, G., Cao, J., and Harley, P.: Effect of isoprene emissions from
807 major forests on ozone formation in the city of Shanghai, China, Atmospheric Chemistry and
808 Physics, 11, 10449–10459, 2011.
809 Geng, F. H., Mao, X. Q., Zhou, M. Y., Zhong, S. Y., and Lenschow, D.: Multi-year ozone
810 concentration and its spectra in Shanghai, China, Science of the Total Environment, 521-522,
811 135-143, 2015.
812 Gery, M. W., and Crouse, R. R.: User's Guide for Executing OZIPR, Atmospheric Research and
813 Exposure Assessment Lab., Office of Research and Development, U.S. EPA, Research Triangle
814 Park, N. C., http://www.epa.gov/scram001/models/other/oziprdme.txt, 2002.
815 Grell, G. A., Peckham, S. E., Schmitz, R., McKeen, S. A., Frost, G., Skamarock, W. C., and Eder, B.:
816 Fully coupled "online" chemistry within the WRF model, Atmospheric Environment, 39,
817 6957–6975,2005.
818 Guenther, A., Karl, T., Harley, P., Wiedinmyer, C., Palmer, P. I., and Geron, C.: Estimates of global
819 terrestrial isoprene emissions using MEGAN (Model of Emissions of Gases and Aerosols from

Nature), Atmospheric Chemistry and Physics, 6, 3181–3210, 2006.
Hong, S. Y. and Lim, J. O. J.: The WRF Single-Moment 6-Class Microphysics Scheme (WSM6), Journal of the Korean Meteorological Society, 42, 129–151, 2006.
Hu, X. M., Klein, P. M., and Xue, M.: Evaluation of the updated YSU planetary boundary layer scheme within WRF for wind resource and air quality assessments, Journal of Geophysical Research-Atmospheres, 118, 10490-10505, 2013.
Hu, X. M., Xue, M., Klein, P. M., Illston, B. G., and Chen, S.: Analysis of Urban Effects in Oklahoma City using a Dense Surface Observing Network, Journal of Applied Meteorology and Climatology, 55, 723-741, 2016.
Lei, W., Foy, B. de, Zavala, M., Volkamer, R., and Molina, L. T.: Characterizing ozone production in the Mexico City Metropolitan Area: a case study using a chemical transport model, Atmospheric Chemistry and Physics, 7, 1347-1366, 2007.
Li, G., Lei, W., Zavala, M., Volkamer, R., Dusanter, S., Stevens, P., and Molina, L. T.: Impacts of HONO sources on the photochemistry in Mexico City during the MCMA-2006/MILAGO Campaign, Atmospheric Chemistry and Physics, 10, 6551–6567, 2010.
Li, G., Bei, N., Tie, X., and Molina, L. T.: Aerosol effects on the photochemistry in Mexico City during MCMA-2006/MILAGRO campaign, Atmospheric Chemistry and Physics, 11, 5169–5182, 2011.
Li, K., Jacob, D. J., Liao, H., Shen, L., Zhang, Q., and Bates, K. H.: Anthropogenic drivers of 2013-2017 trends in summer surface ozone in China, PANS, 116, 2, 422-427, 2019.
Lin, X., Trainer, M., and Liu, S. C.: On the nonlinearity of the tropospheric ozone production, Journal of Geophysical Research Atmospheres, 93 (D12), 15879–15888, 1988.
Lin, Y. F., Wang, Q., Fu, Q. Y., Duan, Y. S., Xu, J. M., Liu, Q. Z., Li, F., and Huang, K.: Temporal-spatial characteristics and impact factors of ozone pollution in Shanghai, Environmental Monitoring in China (in Chinese), 33, 4, 60-67, 2017.
Lin, Y. L., Farley, R. D., and Orville, H. D.: Bulk parameterization of the snowfield in a cloud model, Journal of Climate and Applied Meteorology, 22, 1065–1092, 1983.
Lu, X., Hong, J., Zhang, L., Cooper, O., Schultz, M., Xu, X., Wang, T., Gao, M., Zhao, Y., and Zhang, Y.: Severe surface ozone pollution in China: A global perspective, Environmental Science &Technology Letters, 5, 487–494, 2018.
Monks, P. S., Archibald, A. T., Colette, A., Cooper, O., Coyle, M., Derwent, R., Fowler, D., Granier, C., Law, K. S., Mills, G. E., Stevenson, D. S., Tarasova, O., Thouret, V., von Schneidemesser, E., Sommariva, R., Wild, O., and Williams, M. L.: Tropospheric ozone and its precursors from the urban to the global scale from air quality to short-lived climate forcer, Atmospheric Chemistry and Physics, 15, 8889–8973, 2015.
Ma, Z., Xu, J., Quan, W., Zhang, Z., Lin, W., and Xu, X.: Significant increase of surface ozone at a rural site, north of eastern China, Atmospheric Chemistry and Physics, 16, 3969–3977, 2016.
Nenes, A., Pandis, S. N., and Pilinis, C.: ISORROPIA: A new thermodynamic equilibrium model for multiphase multicomponent inorganic aerosols, Aquatic Geochemistry, 4, 123–152, 1998.
Ran, L., Zhao, C., Geng, F., Tie, X., Tang, X., Peng, L., Zhou, G., Yu, Q., Xu, J., and Guenther, A.: Ozone photochemical production in urban Shanghai, China: analysis based on ground level observations, Journal of Geophysical Research Atmospheres, 114, D15301, 2009.
Sillman, S.: The use of NOy, H2O2, and HNO3 as indicators for ozone-NOx-hydrocarbon sensitivity in urban locations, Journal of Geophysical Research Atmospheres, 100, 14175–14188, 1995.

Sillman, S.: The relation between ozone, NO_x and hydrocarbons in urban and polluted rural environments, Atmospheric Environment, 33, 1821–1845, 1999.

Song, J., Lei, W., Bai, N., Zavala, M., de Foy, B., Volkamer, R., Cardenas, B., Zheng, J., Zhang, R., and Molina L. T.: Ozone response to emission changes: a modeling study during the MCMA-2006/MILAGRO Campaign, Atmospheric Chemistry and Physics, 10, 3827-3846, 2010

Stockwell, W. R., Middleton, P., Chang, J. S., and Tang, X.: The second generation regional acid deposition model chemical mechanism for regional air quality modeling, Journal of Geophysical Research Atmospheres, 95, 16343–16367, 1990.

Sun, L., Xue, L., Wang, T., Gao, J., Ding, A., Copper, O., Lin, M., Xu, P., Wang, Z., Wang, X., Wen, L., Zhu, Y., Chen, T., Yang, L., Wang, Y., Chen, J., and Wang, W.: Significant increase of summertime ozone at Mount Tai in central eastern China, Atmospheric Chemistry and Physics, 16, 10637–10650, 2016.

Tai, A. P. K., Martin, M. V., and Heald, C. L.: Threat to future global food security from climate change and ozone air pollution, Nature Climate Chang, 4, 817–821, 2014.

Tang, G., Li, X., Wang, Y., Xin, J., and Ren, X.: Surface ozone trend details and interpretations in Beijing, 2001–2006, Atmospheric Chemistry and Physics, 9, 8813–8823, 2009.

Tang, W. Y., Zhao, C. S., Geng, F. H., Peng, L., Zhou, G. Q., Gao, W., Xu, J. M., and Tie, X. X.: Study of ozone "weekend effect" in Shanghai, Science in China Series D: Earth Sciences, 51, 9, 1354-1360, 2008.

Tie, X., Brasseur, G., Emmons, L., Horowitz, I., and Kinnison, D.: Effects of aerosols on tropospheric oxidants: a global model study, Journal of Geophysical Research Atmospheres, 106, 22931–22964, 2001.

Tie, X., Madronich, S., Walters, S., Zhang, R. Y., Rasch, P., and Collins, W.: Effect of clouds on photolysis and oxidants in the troposphere, Journal of Geophysical Research Atmospheres, 108, 4642, doi:10.1029/2003jd003659, 2003.

Tie, X., Madronich, S., Li, G., Ying, Z., Zhang, R., Garcia, A., Taylor, J., and Liu, Y.: Characterizations of chemical oxidants in Mexico City: A regional chemical dynamical model (WRF-Chem) study, Atmospheric Environment, 41, 1989-2008, 2007.

Tie, X., Geng, F. H., Peng, L., Gao, W., Zhao, C. S.: Measurement and modeling of O_3 variability in Shanghai, China: application of the WRF-Chem model, Atmospheric Environment, 43, 4289–4302, 2009a.

Tie, X., Madronich, S., Li, G., Ying, Z., Weinheimer, A., Apel, E., and Campos, T.: Simulation of Mexico City plumes during the MIRAGE-Mex field campaign using the WRF-Chem model, Atmospheric Chemistry and Physics, 9, 4621-4638, 2009b.

Tie, X., Geng, F., Guenther, A., Cao, J., Greenberg, J., Zhang, R., Apel, E., Li, G., Weinheimer, A., Chen, J., and Cai, C.: Megacity impacts on regional ozone formation: observations and WRF-Chem modeling for the MIRAGE-Shanghai field campaign, Atmospheric Chemistry and Physics, 13, 5655–5669, doi:10.5194/acp-13-5655-2013, 2013.

Wang, H. J., and Chen, H. P.: Understanding the recent trend of haze pollution in eastern China: roles of climate change, Atmospheric Chemistry and Physics, 16, 4205–4211, 2016

Wang, T., Xue, L., Brimblecombe, P., Lam Y. F., Li, L., and Zhang, L.: Ozone pollution in China: A review of concentrations, meteorological influences, chemical precursors, and effects, Science of Total Environment, 575, 1582-1596, 2017.

Wesely, M. L.: Parameterization of surface resistances to gaseous dry deposition in regional-scale

numerical models, Atmospheric Environment, 23, 1293–1304, 1989.
Xu, J. M., Yan, F. X., Xie, Y., Wang, F. Y., Wu, J. B., and Fu, Q. Y.: Impact of meteorological conditions on a nine-day particulate matter pollution event observed in December 2013, Shanghai, China, Particuology, 20, 69–79, 2015.
Xu, J. M., Chang, L. Y., Yan, F. X., and He, J. H.: Role of climate anomalies on decadal variation in the occurrence of wintertime haze in the Yangtze River Delta, China, Science of the Total Environment, 599-600, 918-925, 2017.
Ying, Z. M., Tie, X., and Li, G. H.: Sensitivity of ozone concentrations to diurnal variations of surface emissions in Mexico City: A WRF/Chem modeling study, Atmospheric Environment, 43, 851–859, 2009.
Zhang, Q., Streets, D. G., Carmichael, G. R., He, K. B., Huo, H., Kannari, A., Klimont, Z., Park, I. S., Reddy, S., Fu, J. S., Chen, D., Duan, L., Lei, Y., Wang, L. T., Yao, Z. L.: Asian emissions in 2006 for the NASA INTEX-B mission, Atmospheric Chemistry and Physics, 9, 5131-5153, 2009.
Zhao, S., Li, J. P., Sun, C.: Decadal variability in the occurrence of wintertime haze in central eastern China tied to the Pacific decadal oscillation, Scientific Reports, 6, 27424, 2016.
Zheng, B., Tong, D., Li, M., Liu, F., Hong, C., Geng, G., Li, H., Li, X., Peng, L., Qi, J., Yan, L., Zhang, Y., Zhao, H., Zheng, Y., He, K., and Zhang, Q.: Trends in China's anthropogenic emissions since 2010 as the consequence of clean air actions, Atmospheric Chemistry and Physics, 18, 14095-14111, https://doi.org/10.5194/acp-18-14095-2018, 2018.
Zhou, G. Q., Xu, J. M., Xie, Y., Chang, L. Y., and Gao, W.: Numerical air quality forecasting over eastern China: An operational application of WRF-Chem, Atmospheric Environment, 153, 94-108, 2017.

Table 1. Statistical analysis on O_3 simulation in September of 2009 by WRF-Chem model compared with measurements of 5 sites (XJH, JS, DT, PD, BS) over Shanghai. MO and MM represent the mean value (unit: ppbv) of observed and modeled O_3 concentration respectively. RMSE and R are the Root Mean Square Error and correlated coefficient respectively calculated between modeled and measured O_3 concentration.

	MO	MM	RMSE	R (99% confidence)
		ppbv		\
XJH	21.6	23.0	7.2	0.78
JS	34.6	30.0	10.3	0.64
DT	47.3	40.3	12.0	0.61
PD	33.5	34.9	8.6	0.74
BS	31.7	31.2	9.3	0.67

Table 2. Statistical analysis on NO_x simulation in September of 2009 by WRF-Chem model compared with measurements of 5 sites (XJH, JS, DT, PD, BS) over Shanghai. MO and MM represent the mean value (unit: ppbv) of observed and modeled NO_x concentration respectively. RMSE and R are the Root Mean Square Error and correlated coefficient respectively calculated between modeled and measured NO_x concentration.

	MO	MM	RMSE	R (99% confidence)
		ppbv		\
XJH	32.1	33.7	7.0	0.74
JS	14.9	14.7	7.6	0.61
DT	3.0	1.5	2.3	0.6
PD	20.3	16.8	7.5	0.82
BS	21.6	16.1	9.8	0.8

Table 3. Scheme of WRF-Chem sensitivity simulations.

Simulation	NO_x EI	VOCs EI	Meteorology
T1 (Control Run)	2009	2009	September of 2009
T2	2015 (30% reduction)	2009	September of 2009
T3	2009	50% increasing	September of 2009
T4	2020 (50% reduction)	2009	September of 2009
T5	2015	50% increasing	September of 2009
T6	70% reduction	2009	September of 2009
T7	2020 (50% reduction)	50% increasing	September of 2009

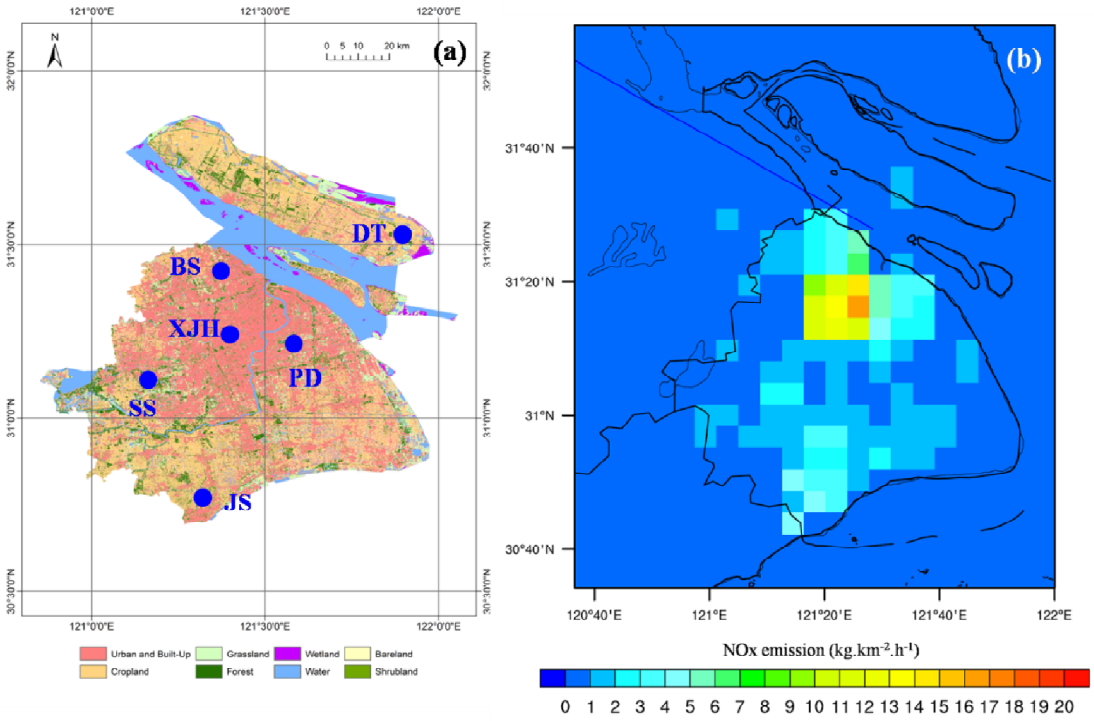

Figure1 (a) The distribution of land-use category in Shanghai. The blue dots denote the locations of 6 sties (XJH, BS, PD, SS, JS, DT). (b) The NOx emission of 2009 scenario in Shanghai.

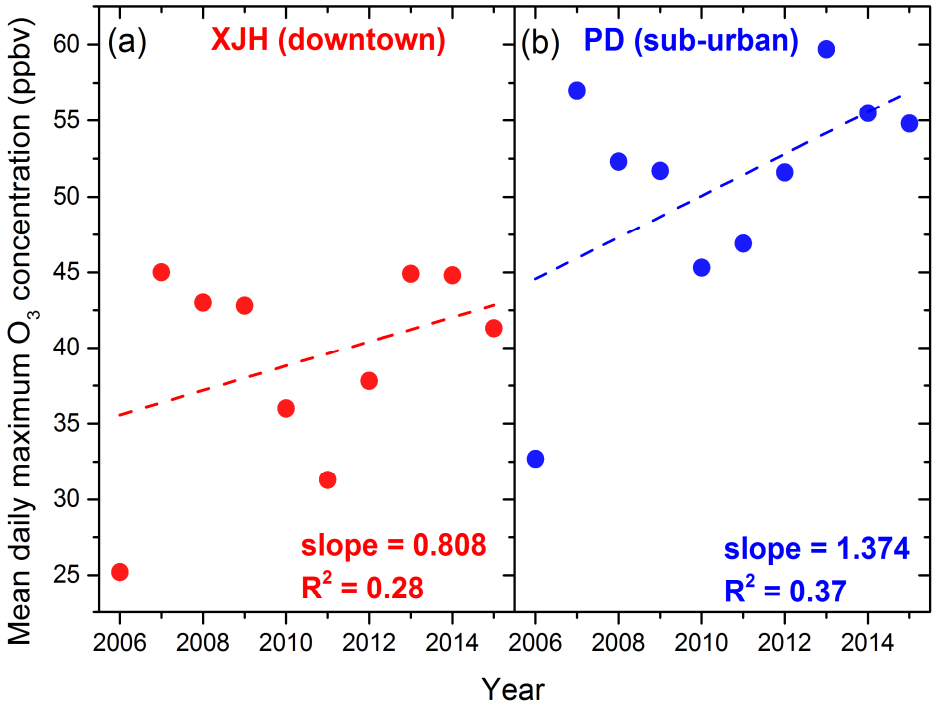

957

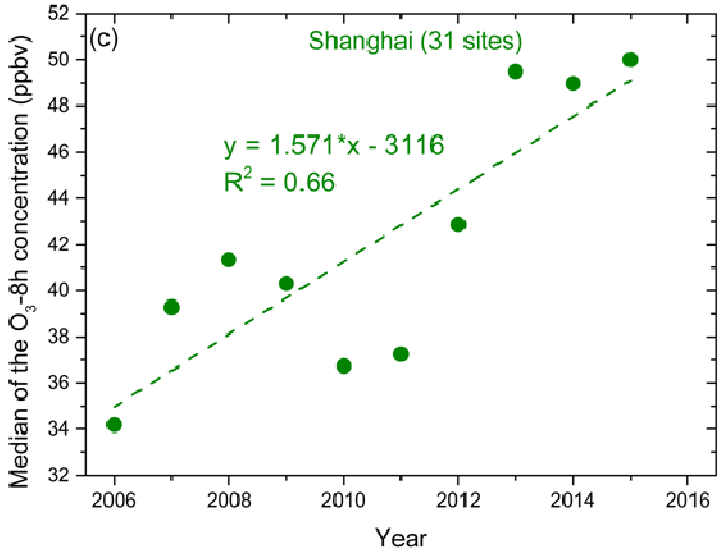

958

959 **Figure 2.** The annual variation of daily maximum O_3 concentration (ppbv) from 2006 to 2015 at (a)
960 downtown site XJH and (b) sub-urban site PD, both presenting the significant increasing trends
961 with 0.808 ppbv yr^{-1} at XJH and 1.374 ppbv yr^{-1} at PD. The variation of the median 8-h O_3
962 concentration (ppbv) from 2006 to 2015 averaged for 31 sites over Shanghai (c), also shows the
963 increasing variability of 1.571 ppbv yr^{-1}.

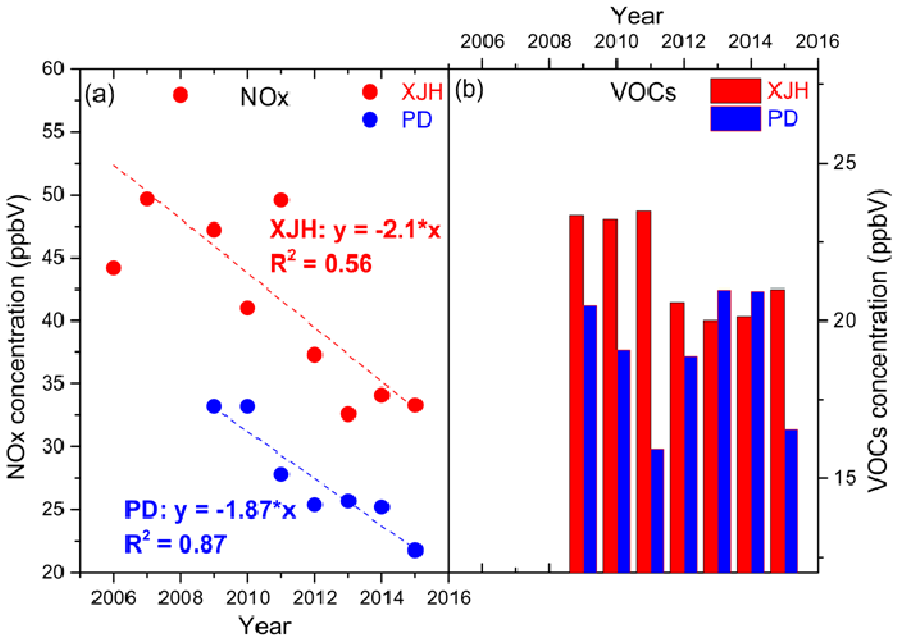

964

965 **Figure 3.** The mean annual concentrations (ppbv) of (a) NO_x (dots) and (b) VOCs (bars) from 2006
966 to 2015 at downtown site XJH and sub-urban site PD respectively. The NO_x concentrations at XJH
967 and PD both present obvious decreasing trends with 2.1 ppbv yr^{-1} and 1.87 ppbv yr^{-1}. While the
968 VOCs concentrations at both sites present no clear inter-annual trends.

969

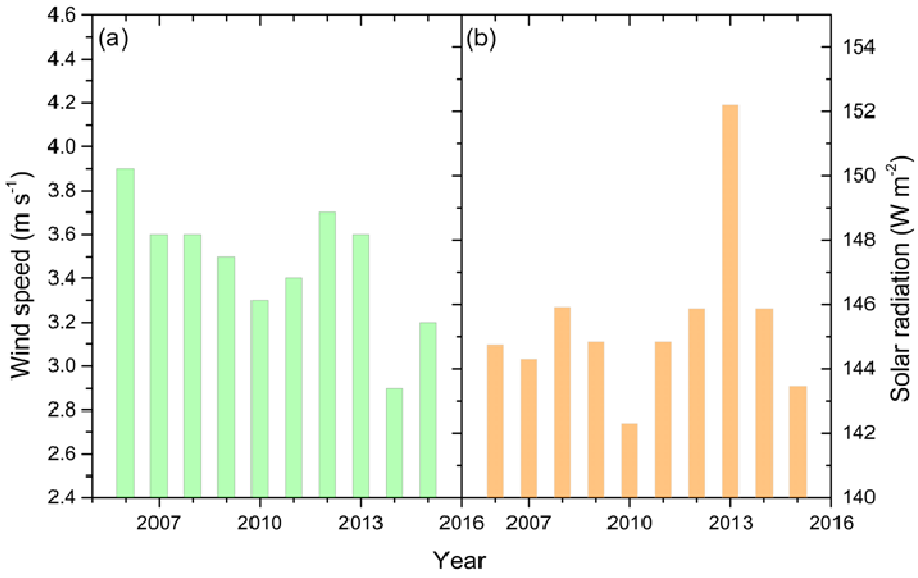

970

971 **Figure 4.** The annual variation of (a) summer wind speed (m s^{-1}) and (b) total solar radiation (W
972 m^{-2}) from 2006 to 2015 in Shanghai. Both wind speed and the solar radiation present weak
973 inter-annual variations but without significant trends.

974

975

976

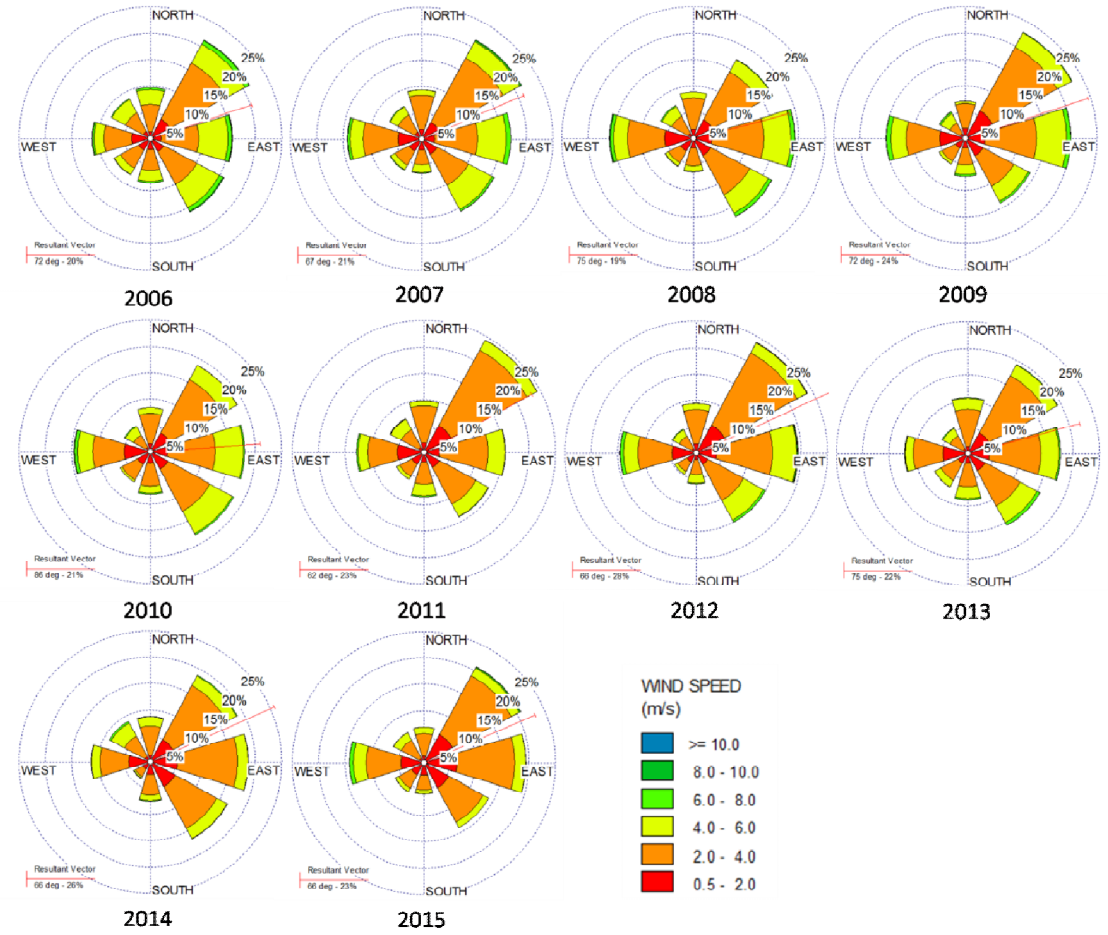

977

978 **Figure 5.** The wind rose of each year from 2006 to 2015 in Shanghai. The red line means the
979 resultant vector suggesting the dominant wind direction.

980

981

982

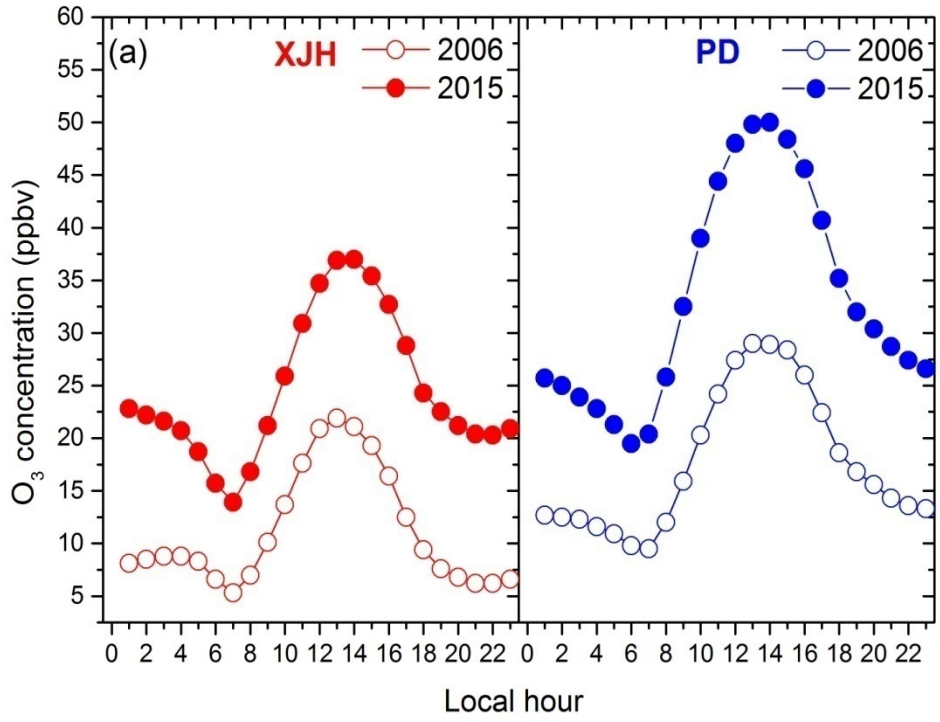

983

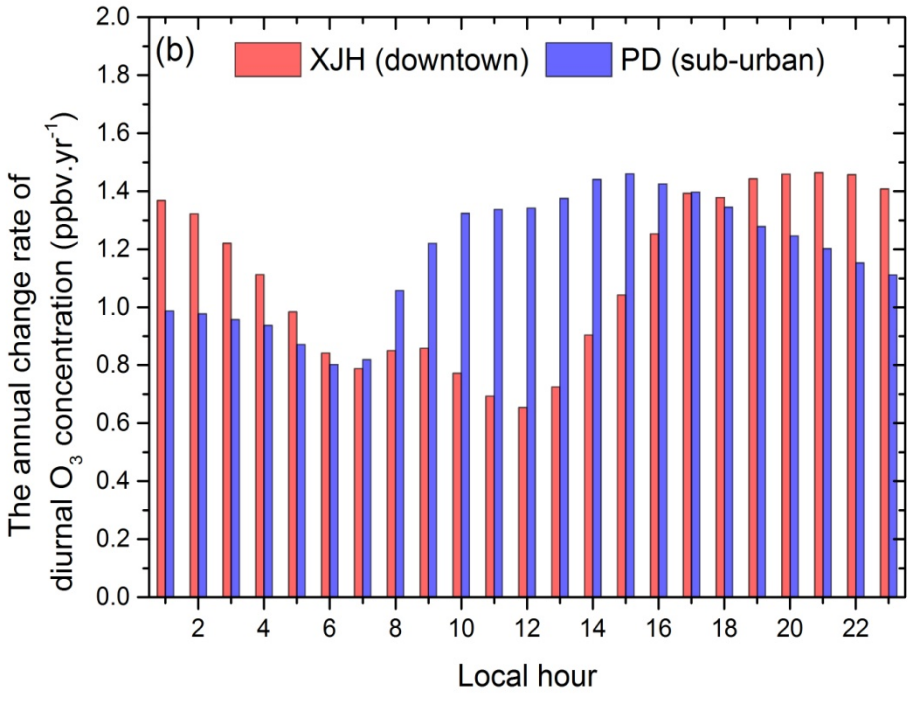

984

985 **Figure 6.** (a) The mean diurnal variation of O_3 concentration (ppbv) compared between 2006 and
986 2015 in XJH (red dots) and PD (blue dots). (b) The annual change rate of diurnal O_3 concentration
987 (ppbv.yr^{-1}) from 2006 to 2015 at downtown site XJH (red bars) and sub-urban site PD (blue bars).
988

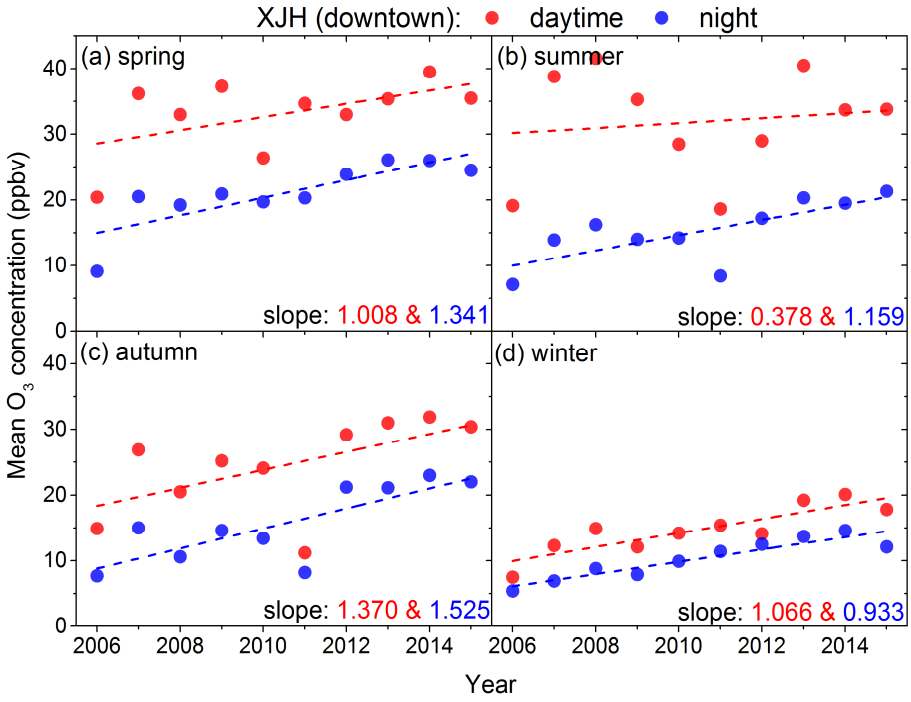

Figure 7. The daytime (8:00-18:00, BJT) and nighttime (19:00-07:00, BJT) O_3 variability from 2006 to 2015 at downtown site XJH in (a) spring, (b) summer, (c) autumn and (d) winter.

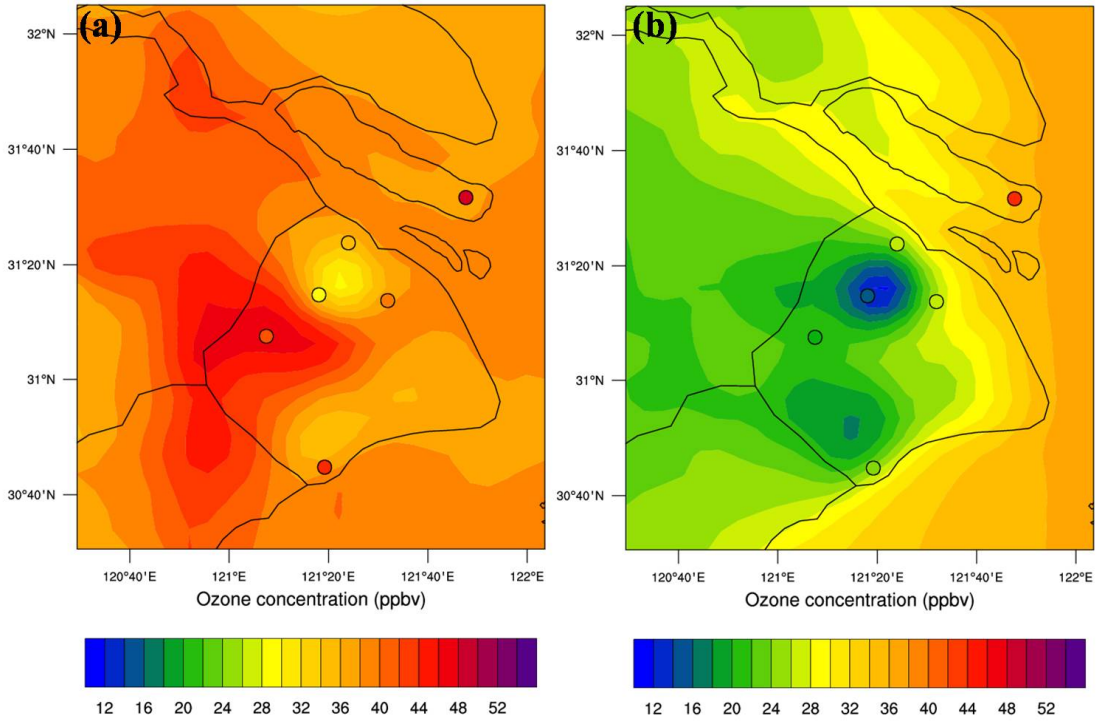

Figure 8. The calculated distribution of (a) daytime and (b) nighttime O_3 concentration by WRF-Chem (shade) in September of 2009 compared with measurements (circles) of 6 sites over Shanghai. The minimum O_3 concentrations in daytime and nighttime both occur in urban center.

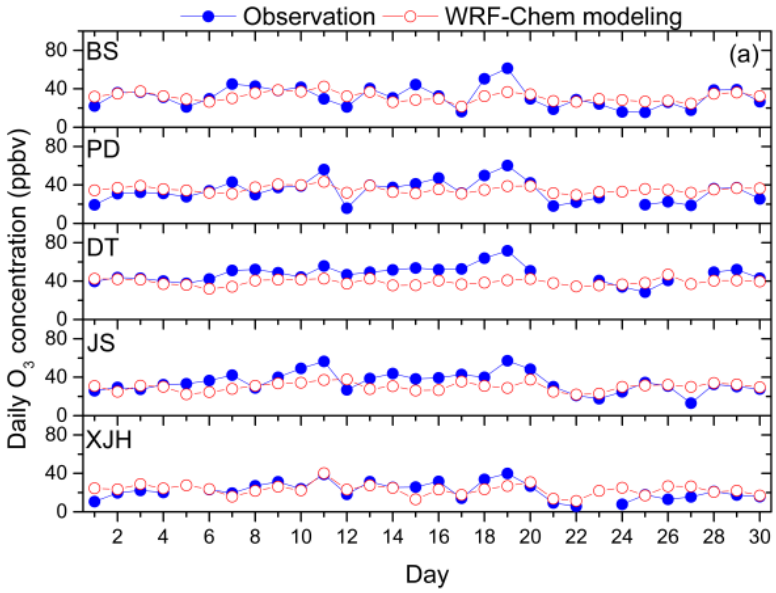

999

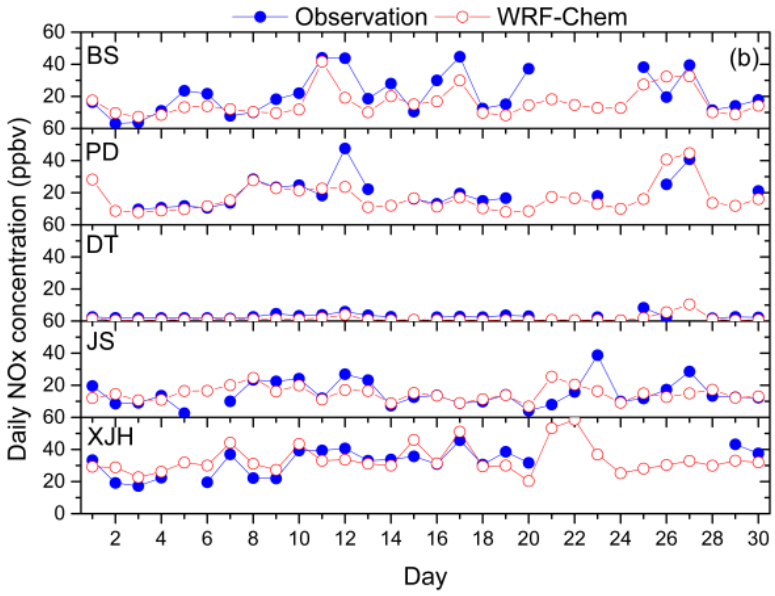

1000

1001 **Figure 9.** The calculated mean daily concentrations (ppbv) of (a) O_3 and (b) NO_x at 5 sites in
1002 September of 2009 by WRF-Chem (red circles) and compared with measurements (blue circles).
1003

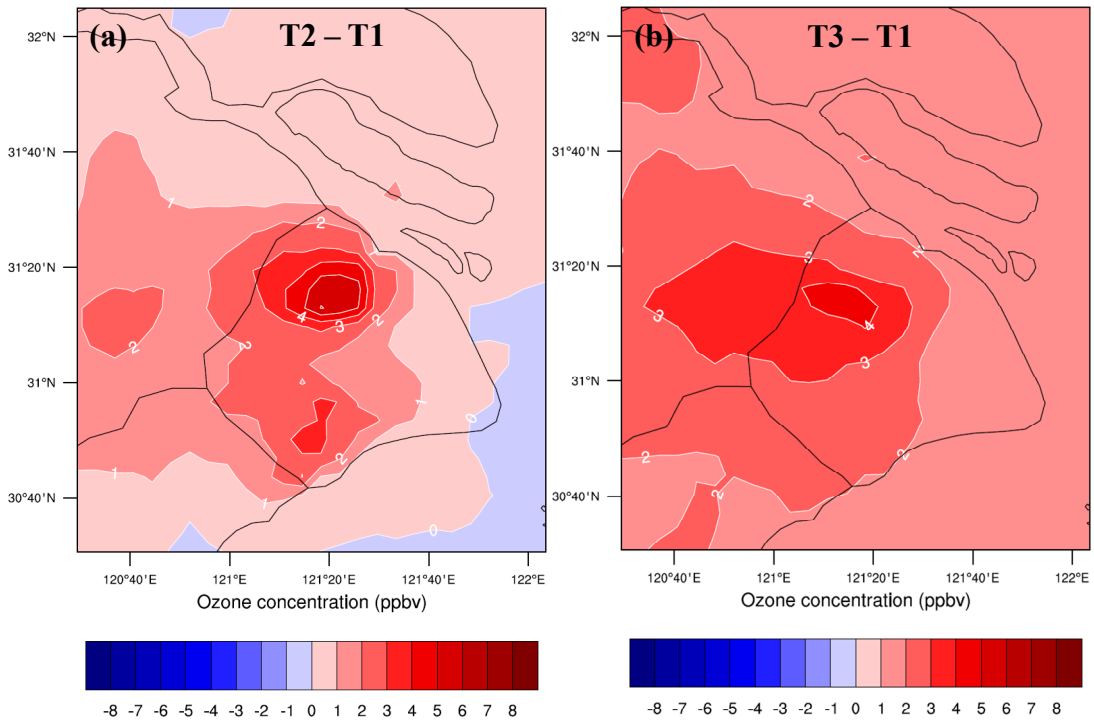

Figure 10. The difference of O3 concentration (ppbv) between (a) T2 and T1 (T2-T1), (b) T3 and T1 (T3-T1) respectively conducted by WRF-Chem model. The difference between T2 and T1 lies in the NO_x emissions set in T2 (2015 scenario) is 30% lower than that in T1 (2009 scenario), which is estimated by Lin et al. (2017) according to the Shanghai Environment Yearbook. The difference between T3 and T1 is dependent on that the VOCs emission in T3 is 50% higher than that in T1.

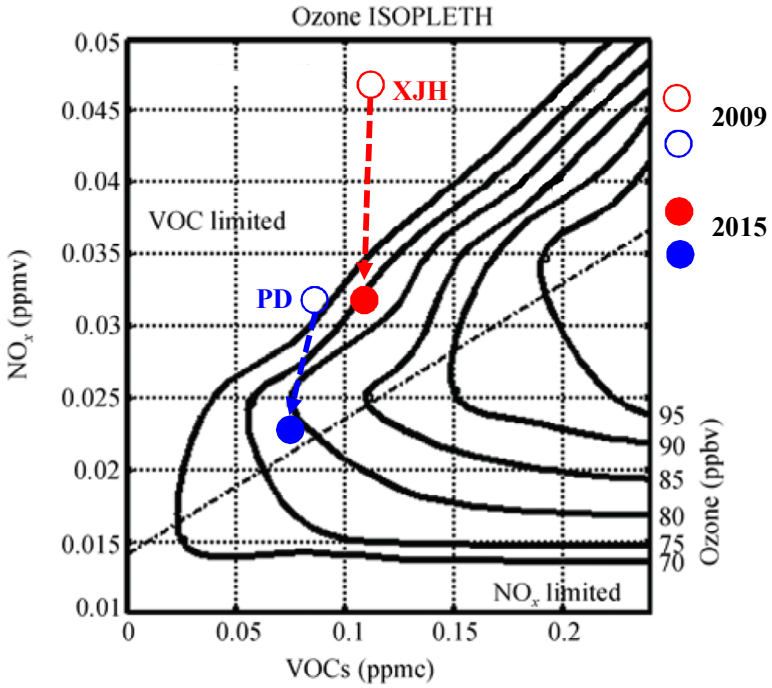

Figure 11. The O_3 chemical production at downtown site XJH and sub-urban site PD in 2009 and 2015 depicted by O_3 isopleths diagram. The hollow and solid red circles denote O_3 production regime at XJH in 2005 and 2019 respectively. The hollow and solid blue circles denote O_3 production regime at PD in 2005 and 2019 respectively

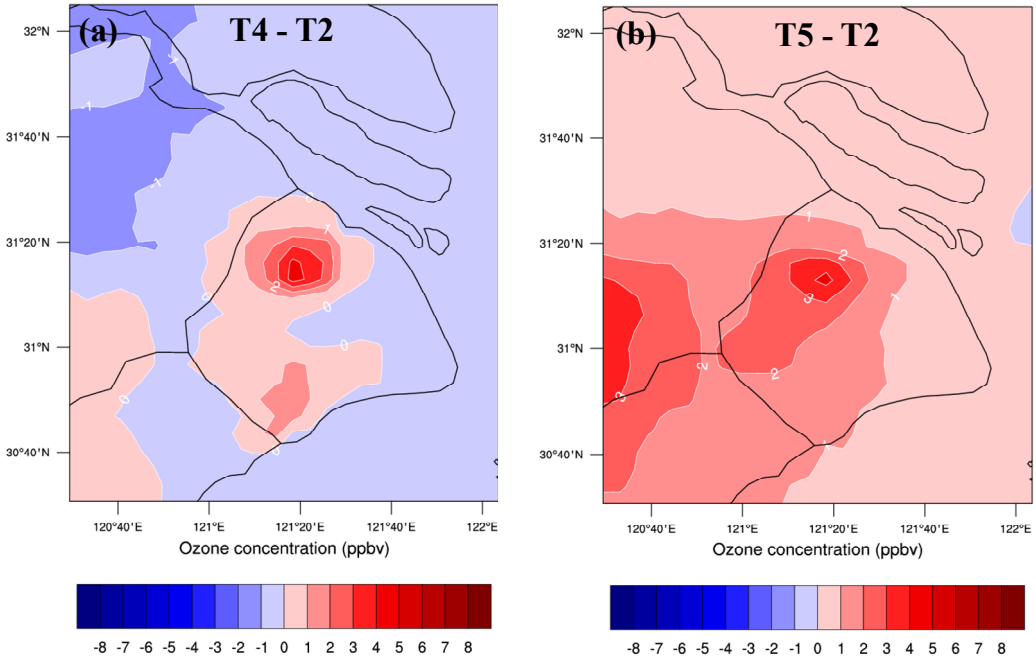

Figure 12. The difference of O3 concentration (ppbv) between (a) T4 and T2 (T4-T2), (b) T5 and T2 (T5-T2) respectively conducted by WRF-Chem model. The difference between T4 and T2 is that the NO_x emissions set in T4 (2020 scenario) is 20% lower than that in T2 (2015 scenario), which is estimated according to the Shanghai Clean Air Action Plan. The difference between T5 and T2 lies in that the VOCs emission in T5 is 50% higher than that in T2.

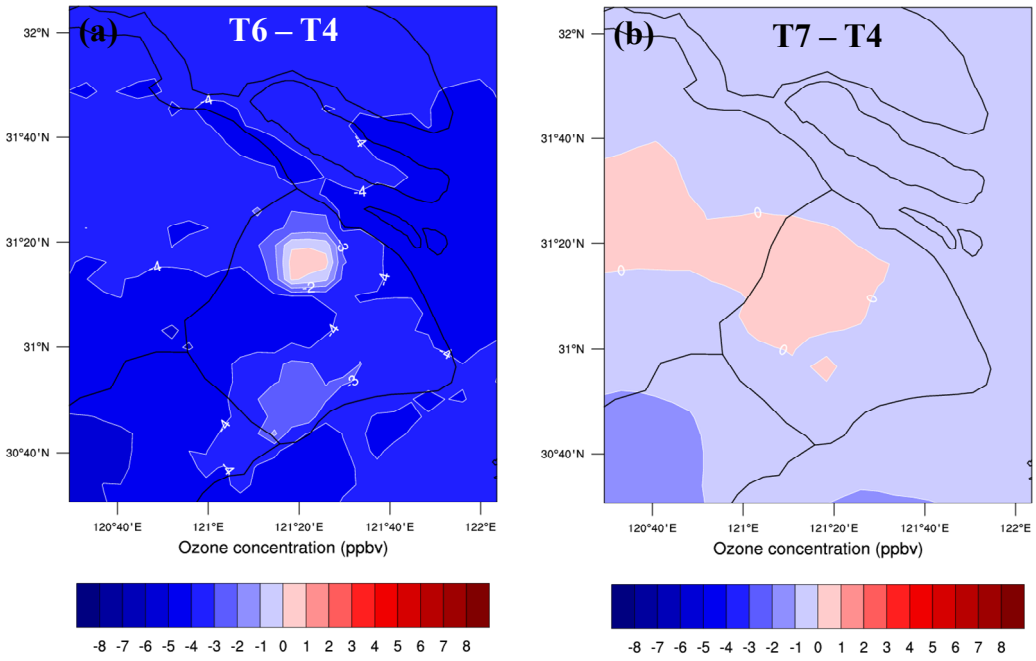

Figure 13. The difference of O3 concentration (ppbv) between (a) T6 and T4 (T6-T4), (b) T7 and T4 (T7-T4) respectively conducted by WRF-Chem model. The NO_x emissions set in T6 is 20% lower than that in T4 (2020 scenario). The VOCs emission in T7 is 50% higher than that in T4.